Università degli Studi di Milano Bicocca
Dept. of Biotechnologies and Biosciences

Ph.D Program in Molecular and Translational Medicine (DIMET)

Long QT Syndrome modelled with human induced pluripotent stem cells

Candidate
Luca Sala
Matricola 700130

Supervisor
Prof. Antonio Zaza, M.D.

Co-supervisor
Dr. Marcella Rocchetti, Ph.D

Cycle XXVII
Academic Year 2013 - 2014

Contents

Chapter 1

Introduction

1.1 Acronyms

ECG	electrocardiogram
AP	action potential
APD	AP duration
SCD	sudden unexpected cardiac death
EAD	early afterdepolarizations
DAD	delayed afterdepolarizations
$\mathbf{I}_{CaL}$	L-type Ca^{2+} current
$\mathbf{I}_{NCX}$	Na^{+}/Ca^{2+} exchanger current
NCX	Na^{+}/Ca^{2+} exchanger
SR	sarcoplasmic reticulum
$\mathbf{Ca}_i$	intracellular Ca^{2+} concentration
$\mathbf{I}_{NaL}$	late Na^{+} current
RyR	ryanodine receptor
SERCA	sarco-endoplasmic reticulum Ca^{2+} ATPase
LQTS	long QT syndrome
$\mathbf{I}_{Kr}$	rapid delayed rectifier K^{+} current

$\mathbf{I}_{Ks}$	slow delayed rectifier K^+ current
TdP	Torsades de Pointes
$\mathbf{I}_{to}$	transient outward K^+ current
RWS	Romano-Ward syndrome
JLNS	Jervell and Lange-Nielsen syndrome
$\mathbf{QT}_c$	corrected QT interval
LCSD	Left Cardiac Sympathetic Denervation
ICD	Implantable Cardioverter Defibrillator
iPS	induced pluripotent stem cells
hiPSC-CMs	human iPS-derived cardiomyocytes
hESC	embryonic stem cells

1.2 Cardiac arrhythmias

Cardiac arrhythmias arise when the myocardium is electrically unstable. They represent a potential life-threatening phenomena, with death often occurring while traveling to the hospital. They are a leading cause of morbidity and mortality, with more than 300,000 people dying every year for arrhythmic sudden unexpected cardiac death (SCD) only in the United States [1]. Unfortunately, SCD may be the first manifestation of the disease as the main cause is often not recognized before death [2]. Alteration in the normal heart rhythm can be observed as changes in the heart rate or in the shape of one or more components of electrocardiogram (ECG). With a slow heartbeat (bradyarrhythmia), the blood pressure cannot be maintained, leading to loss of consciousness and, if prolonged, death. In the same way, when the heartbeat is too fast (tachyarrhythmia), blood pressure cannot be sustained, thus causing syncopal episodes [3]. Cardiac arrhythmias are referred as ventricular when the focus is localized in ventricles [4]. One of the most important al well described form of ventricular arrhythmic syndrome is the long QT syndrome (LQTS) [5].

1.3 Long QT Syndrome (LQTS)

LQTS is an heterogeneous disorder of myocardial repolarization characterized by a prolongation of QT interval on the ECG and clinically manifested with episodes of syncope, seizures and SCD [5][6] as consequences of physical or emotional stress [7].

1.3.1 Causes

A pathological QT interval prolongation mainly originates from 1) genetic causes or 2) acquired causes [8].

1.3.1.1 Congenital LQTS

The inclusion of a genetic substrate in the development of cardiac arrhythmias provided new insights in the comprehension of cardiac electrophysiology [9]. Genetic alterations may be primarily manifested as mutations in genes related to the electrical and contractile machinery of the heart, as ion channels, contractile proteins and proteins involved in Ca^{2+} signaling and compartmentalization [9].

Classification and epidemiology Two main hereditary variants of LQTS have been described: the most common, autosomal dominant, Romano-Ward syndrome (RWS), described in 1963 [10] and the extremely severe, autosomal recessive, Jervell and Lange-Nielsen syndrome (JLNS), characterized by loss of function in slow delayed rectifier K^+ current (I_{Ks}) and associated with congenital deafness because of the failing endocochlear K^+ cycling required for normal hearing [11].

Nowadays, mutations in 13 genes tuning the cardiac action potential have been found directly responsible for LQTS (table 1.1). The first three genes identified associated with LQTS were KCNQ1, KCNH2 and SCN5A; overall, they are the most frequent variants (LQT1 - LQT3) and account for almost 90% of all LQTS cases [12][13]. Other genes were linked to LQTS but they are defined of minor (LQT4 - LQT13) susceptibility since they account only for 5% of the cases [14].

In the past, LQTS was accounted to have a prevalence between 1:5,000 up to 1:20,000 births without any supporting data. However, in 2009, a multicenter study on 44,596 infants at 3-4 weeks of age clearly demonstrated that the prevalence of LQTS is close to 1:2,000 healthy-live births [15], classifying LQTS at the edge of orphan diseases.

Type	Gene	Syndrome	Frequency (%)	Functional effect
LQT1	KCNQ1	RWS, JLNS	40-55	$K_V7.1$ (↓)
LQT2	KCNH2	RWS	30-45	$K_V11.1$ (↓)
LQT3	SCN5A	RWS	5-10	$Na_V1.5$ (↑)
LQT4	ANKB	RWS	<1%	Ankyrin B (↓)
LQT5	KCNE1	RWS, JLNS	<1%	MinK (↓)
LQT6	KCNE2	RWS	<1%	MiRP1 (↓)
LQT7	KCNJ2	AS	<1%	$K_{ir}2.1$ (↓)
LQT8	CACNA1c	TS	<1%	$Ca_V1.2$ (↑)
LQT9	CAV3	RWS	<1%	Caveolin 3 (↓)
LQT10	SCN4B	RWS	<1%	Na^+ channel $\beta 4$ (↓)
LQT11	AKAP9	RWS	<1%	Yotiao (↓)
LQT12	SNTA1	RWS	<1%	Syntrophin-$\alpha 1$ (↓)
LQT13	KCNJ5	RWS	<1%	$K_{ir}3.4$ (↓)

Table 1.1: LQTS genes. RWS: Romano-Ward syndrome; JLNS: Jervell-Lange-Nielsen syndrome; AS: Andersen syndrome; TS: Timothy syndrome; Functional effect: (↓) loss-of-function or (↑) gain-of-function at cellular in vitro level. Adapted from [12].

Role of modifier genes LQTS is characterized by clinical heterogeneity, therefore members of the same family with a common mutation have different degrees of disease severity. Usually, this is attributed to the variable penetrance of the disease but, recently, genetic modifiers have been shown to play a pivotal role in shaping the disease traits [16]. The role of genetic modifiers in congenital LQTS has been increasingly recognized, since they represent an important source of variations which strongly alter the clinical phenotype in addition to the effect of the primary mutation [17]. The clinical evaluation of founder population is extremely useful in these cases since members share the same mutation but can experience profoundly different phenotypes [18]. Common single nucleotide polymorphisms (SNP) in ion channel genes, as KCNQ1, KCNH2, KCNE1, KCNE2, have been found associated with an increased arrhythmia susceptibility in LQTS cohorts [16][18][19]. Additionally, genes unrelated to ion channels have been attributed the role of genetic modifiers. For example, SNP in NOS1AP [17] specifically worsen the arrhythmogenic phenotype of $KCNQ1^{A341V}$ mutation in term of risk for cardiac events. Furthermore, SNP in AKAP9 have been related to an increased disease severity and prominent corrected QT interval (QT_c) prolongation [20]. Surprisingly, other SNP in the AKAP9 exert an opposite effect by blunting the impact of the primary mutation and profoundly altering the genotype-phenotype correlation of these populations [20]. Furthermore, genes associated with the β-adrenergic cascade as ADRA2C (α2-adrenergic receptor) and ADRB1 (β1-adrenergic receptor) have been associated with a worsening in the clinical phenotype due to an increased sympathetic activity [21]. With the rapid growth of new diagnostic techniques, it will be possibile to increase the informations available on the correlation between the genetic background of the patient and its clinical phenotype.

1.3.1.2 Acquired

Acquired LQTS constitutes a pathological prolongation of QT interval induced by damaging stimuli, which returns to normal values once the stressor is removed [8]. Drugs and preexisting physiological or pathological conditions are the two major players in QT interval prolongation in acquired LQTS.

Drugs in the 60's, the correlation between congenital LQTS and ion channel mutations [10][11] led to the logical conclusion that also pharmacological agents targeting ion channels were able to trigger a LQTS phenotype. The most striking example of this correlation is the high susceptibility of rapid delayed rectifier K^+ current (I_{Kr}) block by specific drugs [22]: the presence of aromatic aminoacids (Tyr^{652} and Phe^{656}, figure 1.1) in the channel pore and the absence of prolines in the drug binding site offer the perfect environment for compound binding to Kv11.1 [8][23]. I_{Kr} is the main responsible for the rapid repolarization during phase 3 of action potential (AP) and its block strongly impairs repolarization and prolongs QT interval (figure 1.2), leading to life-threatening arrhythmogenic events like Torsades de Pointes (TdP) (figure 1.2).

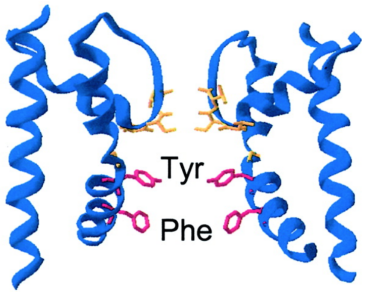

Figure 1.1: Structural localization of Tyr^{652} and Phe^{656} in the S6 domain of I_{Kr}. Adapted from [23].

This findings had a huge relevance in drug development and testing [24]. In 1997, the Committee for Proprietary Medicinal

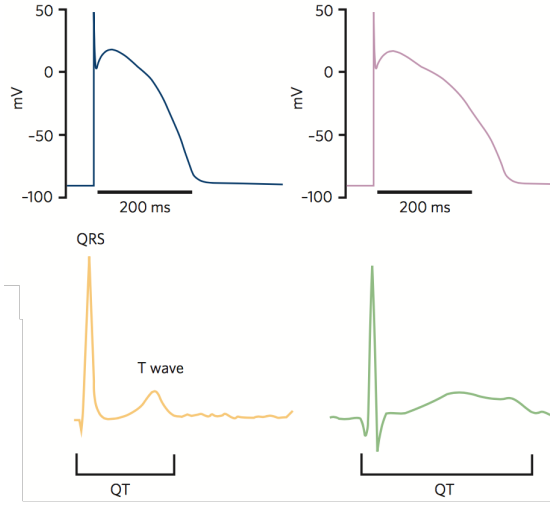

Figure 1.2: Effect of I_{Kr} block on action potential (left) and QT (right). Adapted from [23].

Products (CPMP) published a document which pointed out recommendations for clinical and non-clinical approaches to study drug-induced QT prolongation, with peculiar references to drug industry [25]. A following study [26] outlined a classification on a 100-drugs subgroup in order to clarify the relationship between drug-induced QT prolongation and I_{Kr} block; although the correlation between I_{Kr} block and TdP is not linear, the risks of developing drug-induced QT prolongation must be taken very seriously during all the stages of drug development, with a particular attention to all the compounds with an high risk-benefit ratio. A 30-fold margin between the IC_{50} for I_{Kr} and the maximum drug concentration administrable was retained adequate to ensure an acceptable degree of safety from TdP, with a low risk of false positives [26]. Economical and practical reasons force companies to put I_{Kr}-block assays in the forefront of preclinical stages of drug development [27]. In particular, the *in vitro* hERG assay actually represents the most used test to predict cardiotoxicity by I_{Kr} block. This test is performed in cell lines transfected with KCNH2 plasmids, and the magnitude of I_{Kr}

is assessed with the patch clamp technique in voltage-clamp configuration. However, recent evidences suggest to extent the concept of this assay to more complex biological systems considering that the lack of predictive power has been demonstrated [28]. Anyway, the clinical phase validation of *in vitro* data with ECG remains essential [27].

Preexisting conditions Other conditions are associated with acquired LQTS, playing the role of risk factors which can raise the probability of QT interval prolongation and subsequent TdP under drug exposure. Sex hormones have been shown to be associated with a 2 to 3 times higher risk of experiencing TdP in women than men [29], in accordance with the evidence that QT shortens after puberty in males but not females [30] in response to I_{Kr} boost by testosterone [31]. I_{Kr} is reduced with low extracellular K^+ concentration because of competitive block by Na^+ ions and enhanced inactivation [32]. In addition, Kv11.1 drug binding site is more exposed in these conditions [33], making hypokalemia a potent QT lengthening factor. Bradycardia is also considered an important risk factor; in human and large mammal myocardium, a slow heart rate significantly prolongs AP duration (APD) by acting on the duration of repolarization [34]. Furthermore, suboptimal activation of transient outward K^+ current (I_{to}) enhances L-type Ca^{2+} current (I_{CaL}) voltage-dependent recovery from inactivation, starting arrhythmogenic events leading to TdP [35]. A minor and certainly particular case is offered by preexisting conditions or environmental factors which can alter drugs pharmacodynamic. The antihistamine *terfenadine*, a potent I_{Kr} inhibitor in its prodrug form, exerts its cardiotoxic action only when not metabolized. Conditions inhibiting or reducing CYP3A function, e.g. as a consequence of drugs, overdose or diseases leads to strong QT prolongations [24].

1.3.2 Consequences

1.3.2.1 Cellular level

The cardiac action potential is generated by the interplay of depolarizing and repolarizing ion movements that flow across cell membrane through ion channels, pumps and exchangers [36] (figure 1.3). Alterations in this process can occur at every level, and the outcome depends on which mechanism is involved.

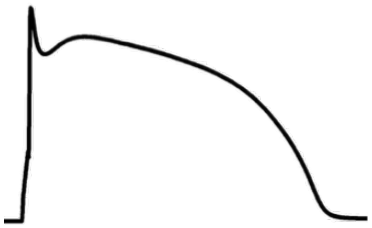

Figure 1.3: Action potential of canine ventricular cardiomyocyte.

One of the most recurrent mechanism of cardiac arrhythmias is the presence of *triggered activity*, i.e. the generation of an electrical impulse as a direct consequence of a prior one [37]. Triggered activity arises mainly by 1) early afterdepolarizations (EAD) or 2) delayed afterdepolarizations (DAD).

An EAD is defined as a reversal of the repolarization during AP [38] (figure 1.4). It can occur as a result of a compromised repolarization reserve, which generates a reduction in the net outward current. In these conditions, any mechanism supporting a net inward current can potentially twist the repolarizing process of AP. During the AP late plateau phase, the synergistic interaction of I_{CaL} and Na^+/Ca^{2+} exchanger current (I_{NCX}) sustains the positive feedback supporting EAD. I_{CaL} *window* region offers the ideal substrate for EAD generation: if the repolarization of the AP is slow (i.e. as a consequence of a reduced K^+ current or increased inward conductance), the time- and voltage-dependent recovery from inac-

tivation of Ca^{2+} channels support I_{CaL} resurgence, generating an EAD. I_{NCX} is the other major player in EAD onset. Na^+/Ca^{2+} exchanger (NCX) is electrogenic, since it exchanges 3 Na^+ ions with 1 Ca^{2+} ion. In *forward* mode, it extrudes Ca^{2+} ions from the cell, generating an inward I_{NCX}. On the opposite, when Na^+ is extruded (*reverse* mode) I_{NCX} is outward. During AP plateau, I_{NCX} is inward as it reflects Ca^{2+} removal from cytosol, thus slowing the repolarization process. In these conditions, if intracellular Ca^{2+} concentration (Ca_i) further increases (e.g. due to I_{CaL} recovery from inactivation or Ca^{2+} releases from the sarcoplasmic reticulum (SR)), I_{NCX} promotes and sustains the generation of an EAD-triggered AP.

I_{NCX} has also a pivotal role in another mechanism of triggered activity: DAD. They constitute membrane potential depolarizations occurring in diastole [39] (figure 1.4). DAD generation starts from SR: in pathological condition as SR-Ca^{2+} overload or excessive Ca^{2+} leak from ryanodine receptor (RyR), spontaneous waves of Ca^{2+} may arise within the cell after the termination of an AP. These sudden diastolic Ca_i increasings generate a net inward I_{NCX} which causes DAD. If the amount of Ca^{2+} released from the SR is remarkable, DAD-triggered AP are generated, thus further feeding triggered activity [40].

1.3.3 Diagnosis

The presence of QT prolongation and syncope after physical or psychological stress make the diagnosis of LQTS very clear for physicians. However, in case of borderline QT prolongation and absence of symptoms, the diagnosis might be more complicated. For this reason, a series of diagnostic criteria was proposed in 1985 [41] by giving different weight to major and minor parameter of evaluation and defined as *Schwartz score*; those principles were updated in

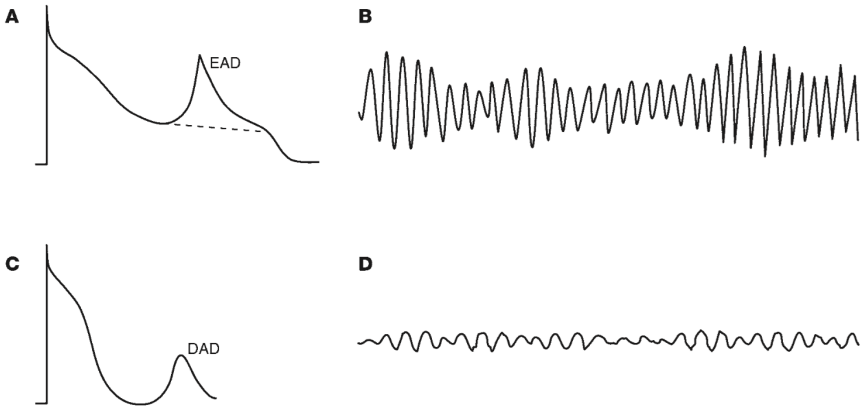

Figure 1.4: Afterdepolarizations and ventricular arrhythmias: *A)* EAD; *B)* ECG with TdP from a polymorphic ventricular tachycardia associated with EAD. *C)* DAD; *D)* ECG of ventricular fibrillation associated with DAD. Adapted from [1].

1993 [42] (table 1.2).

As a complementary tool for these criteria, genetic screening has now become essential in the diagnosis of borderline cases and to identify potential silent mutations in family members [43].

1.3.4 Genotype-phenotype correlation

Since the discovery of the first three LQTS genes in the 90's (i.e. KCNQ1, KCNH2, SCN5A), it was clear that LQTS could represent a powerful model for the study of genotype-phenotype correlation. The first step towards this correlation was made by a study in 1995, in which it was demonstrated that distinctive T wave patterns can be correlated with each of the three genes of LQTS [45]. This suggested that the the prolongation of cardiac repolarization was only a common trait of different genetic modifications , which should be rather considered as different entities [46]. From this point, genotype-phenotype correlation acquired a pivotal role in both diagnosis and treatment of LQTS patients. Symptomatic mutations in the first three key genes were also correlated

ECG findings	Points
QTc	
>480 ms	3
460-479 ms	2
450-459 (male) ms	1
QTc 4^{th} minute of recovery from exercise stresss test ≥480 ms	1
TdP	2
T-wave alternans	1
Notched T wave in 3 leads	1
Low heart rate for age	0.5
Clinical history	
Syncope with stress	2
Syncope without stress	1
Congenital deafness	0.5
Family history	
Family members with definite LQTS	1
Unexplained SCD below age 30 amongst immediate family members	0.5

Table 1.2: 1993-2012 LQTS diagnostic criteria: *Schwartz score*. Score <1 point: low probability of LQTS; 2-3 points: intermediate probability; ≥ 3.5 points: high probability. Adapted from [43][44].

with gene-specific triggers for the initiation of life-threatening arrhythmias as physical exercise (LQT1), emotional stress (LQT2) or rest/sleep (LQT3) [47]. Later works pinpointed swimming [48] and auditory stimuli [49] as key events respectively for LQT1 and LQT2. Another breakthrough on the genotype-phenotype correlation in LQTS is the discovery that the localization of KCNQ1 [50] and KCNH2 [51] mutations can be predictors of the severity of the disease; mutations in the transmembrane region of both channels have been demonstrated as more malignant than mutations in other spots [46]. This allowed the correlation of malignant manifestations with a particular genetic background. Beyond this correlations, in recent years the problem of quantifying LQTS penetrance increased its relevance. LQTS was previously attributed a penetrance close to 90% but some authors proposed in early 80's that the spectrum of the disease could have been much larger, even involving individuals with a normal QT interval [52]. A following study on 5 LQTS families confirmed this hypothesis, highlighting the presence of kin in which the penetrance of the disease settled around 25-35%. These individuals tested positive for the mutation, but experienced normal or borderline QT intervals, probably due to the counteracting effects of genetic background or genetic modifiers; without the contribution of molecular diagnosis, these subject would have been considered healthy. However, this condition puts them at risk, with an concrete chance to develop drug-induced arrhythmogenic events [52]. Electrophysiological in vitro data have broaden this concept: the functional consequences mutations in the same gene can vary substantially. This is particularly true for K^+ channels, which requires the coassembly of α-subunit with an unknown number of function-modifying β-subunit; functional channels can then be constituted by both wild type and mutant subunits in different combinations, which could interfere with genotype-phenotype

correlations [53].

1.3.5 Current therapies

The therapy for LQTS is mainly constituted by the combination of β-adrenergic blocking agents, Left Cardiac Sympathetic Denervation (LCSD) and Implantable Cardioverter Defibrillator (ICD). Other pharmacological therapies are used in support to the standard, but the choice is currently very limited [54].

1.3.5.1 β-blockers

They represents the gold standard agent for the treatment of symptomatic patients. They prevent the pathogenic increase in I_{CaL} under β-adrenergic stimulation without sensibly altering the heart rate in the majority of patients [55]. For this reason, they are extremely effective in LQT1 patients, with a reduction of approx. 97% of life-threatening cardiac events [56]. In LQT2 patients, β-blockers are less effective, but they still represent the first choice therapy [56]. Adult LQT3 patients evidenced instead a good response to the therapy, with a low mortality rate including only patients with extremely prolonged QT intervals [54].

1.3.5.2 Left Cardiac Sympathetic Denervation (LCSD)

In patients where the β-blocker therapy is not effective, LCSD represent the second choice for the treatment. LCSD is the removal of the first four thoracic ganglia, generating a substantial reduction of noradrenaline release at ventricular level without decreasing the heart rate [57]. LCSD induces also a significative shortening of QT_c, as a consequence of the decreased sympathetic activity targeting ventricles. This shrinks the occurrence of life-threatening cardiac events in patients resilient to a full dosage of β-blocker therapy [54].

1.3.5.3 Implantable Cardioverter Defibrillator (ICD)

The ICD is a device surgically placed in the chest of the patient that generates electrical shocks to restore the normal electrical activity during arrhythmias. Clinicians prefer to implant an ICD to cautelate themselves from the risk of potential medicolegal consequences following SCD. However, its application is recommended with recurring cardiac arrests on a correct or full dose drug therapy and only after considering LCSD as second choice [54][58].

1.4 Induced pluripotent stem cells

In recent years, the need for good and reliable experimental *in vitro* models reached a new level in term of importance. To reproduce specific feature of human diseases has become extremely challenging, since almost every model available recapitulate only a few traits of the disease [59]. In addition, obtaining human samples for ex vivo studies can be particularly challenging if not impossibile for many tissues. Embryonic stem cells (hESC) did represent the gold standard in term of pluripotency and differentiation capabilities for studies on human derived samples since they are obtained from the inner core of a blastocyst. However, the handling of embryonic material raises, even today, many ethical and moral concerns on the fact that embryos should or not be attributed the moral status of fully grown individuals. In 2006, the first proof that somatic cells could be reprogrammed to acquire pluripotency features, introduced a new competitor in the field of reprogramming biology. These new cells, defined as induced pluripotent stem cells (iPS), possess all the properties of hESC, as the ability to grow indefinitely and to differentiate virtually into a high number of somatic cells of the body. This is achieved by using specific protocols to drive the differentiation of iPS cells towards different cell types. At present

day, iPS have been differentiated into neurons, hematopoietic cells, hepatocytes, smooth muscle cells and cardiomyocytes (human iPS-derived cardiomyocytes (hiPSC-CMs)) [60][61]. Different strategies are currently used: the most exploited recreates the differentiation events happening in vivo during development, by agonizing or antagonizing signaling pathways with specific compounds. Another approach, instead, requires the use of co-culture systems as a feeder layer for supplying growth factors. Other techniques supply iPS with specific defined factors combined with protein integration [62][63][64]. The ability of generating patient-specific cells without the use of the highly inefficient and ethically controversial *somatic cell nuclear transfer* [65], transformed this strategy in the state-of-the-art of disease models. This cell types allows the study of diseases within the genetic background of patients; this means that in addition of the disease mechanism, it is also possible to investigate the role of the genetic background in shaping the disease traits or, for example, in drugs response. This is even more important for tissue which are extremely hard to obtain, like neurons or ventricular cardiomyocytes. However, cell maturity must be taken into account for modeling human diseases: many of them develops over time under the persistent presence of environmental, physiological or pathological stimulus or, otherwise, they require a specific maturation stage to be reached. For monogenetic diseases that evidence cell-autonomous defects, as ion channel mutations, iPS represent instead the most suitable cellular model available [66]. Furthermore, strong validations are emerging by using iPS assays for drug discovery and toxicity [67], but further and independent confirmations are required before acceptance from regulatory authorities. The main issues of iPS concerns the reprogramming procedure, not necessary for hESC, which can lead to consistent accumulation of mutations. This can be particularly problematic for the comparison

of pathological phenotypes with healthy donors, because the effects of mutations acquired during the reprogramming process sum up to the intrinsic biological variability. Also, issues can emerge by subtle differences in silencing the expression pattern of somatic cells from which they are derived, i.e. the epigenetic memory [68]. This is confirmed by the comparison of differentially methylated regions, which clearly separated iPS population from both hESC and their somatic origin [69]. In addition, strategies of reprogramming (table 1.3) could introduce a consistent amount of genomic modification strongly increasing the heterogeneity within the cell population.

1.4.1 Differentiation methods

The first achievement of reprogramming human somatic cells to iPS was obtained by two independent groups in 2007 by the expression of four transcription factors: OCT4 and SOX2, in combination with either KLF4 and MYC [70] or NANOG and LIN28 [71]. The original methods for the generation of iPS used retroviral vectors as a carrier for the reprogramming genes, which are silenced after the infection of dividing cells; this approach still remains the most common. Another integrating technique make use of lentiviral vectors which infects both dividing and non dividing cells [72] and can be implemented with inducible or recombinase-excisable systems; however, fragments from the viral constructs might remain integrated into the genome after removing the sequences of the viral construct. The most recent techniques focus on the avoidance of insertional mutagenesis or transgene silencing, boosting the reliability and reproducibility of the generated cell lines [66]. However, with the actual technologies, these non-viral and non-integrating approaches are limited by the low efficiency of iPS generation.

Method of reprogramming	Delivery method
Integrating	
Viral	Retrovirus
	Lentivirus
Non-viral	Transposon
Non-integrating	
Viral	Adenovirus
	Sendai virus
Non-viral	mRNA
	miRNA
	Small molecules
	Episomal vectors
	Proteins

Table 1.3: Methods for the delivery of reprogramming factors. The most used methods are highlighted in gray. Novel and non integrating methods which have been recently implemented in many laboratories are highlighted in orange. Adapted from [66].

1.4.2 Comparison with other experimental models

The need of a good and reliable experimental model, able to reproduce the key features of human diseases, is always been extremely important in life sciences. For the study of molecular mechanisms of cardiac diseases, two main experimental approaches are currently used: 1) studies in heterologous systems and 2) animal models. The first approach is mainly used to investigate the function and the localization of specific proteins without considering the physiological environment. This is extremely useful in case of mutation in ion channels; the mutated gene is inserted within a plasmid and transfected into cells which have a low background electrical activity. In this way, since the transfected mRNA is overexpressed, the ion channel structure and function can be investigate without any other major interference. Downsides include the absence of a proper physiological environment to study the indirect consequences of the mutation on overall cell functions. Furthermore, they lack the pos-

sibility of simulating a whole-heart condition, which is actually possible for iPS by the use of embryoid bodies (EB) in MultiElectrode Array (MEA). Animal models, instead, represent a total different reality. They are extremely useful and still necessary to investigate and explore novel biological insights, but these system presents some concerns; first of all, they are extremely expensive when compared to in vitro studies. In addition, reproducing the traits of human diseases in animals can be particularly challenging considering the different genetic background and the fact that, although macroscopic functions are conserved, microscopic ones might differ consistently.

In this context, iPS represents a breakthrough both for the discovery of novel biological targets and for the promising patient-specific therapeutic applications.

1.5 Scope of the thesis

The aim of this work is the in vitro characterization of two LQTS mutations in patient-specific hiPSC-CMs to evaluate the arrhythmogenic mechanisms and genotype-phenotype correlations. Functional characterizations were performed on both EB and isolated hiPSC-CMs. The mutation CALM1^{F142L}, presented in chapter 2, is a recently discovered de novo mutation in CALM1 gene associated with recurrent cardiac arrest in infants. We evaluated the arrhythmogenic mechanism underlying this severe LQTS mutation. The mutation KCNQ1^{Y111C}, discussed in chapter 3, is a well known LQTS mutation originated from a Swedish founder population and associated with increased arrhythmia susceptibility and SCD. We validated hiPSC-CMs as an LQTS model for a mutation which evidenced a mild clinical phenotype despite displaying a severe loss of function in vitro.

1.6 References

1. George, A. L. Molecular and genetic basis of sudden cardiac death. *J. Clin. Invest.* **123,** 75–83 (Jan. 2013).
2. John, R. M., Tedrow, U. B., Koplan, B. A. & Albert, C. M. Ventricular arrhythmias and sudden cardiac death. *The Lancet* **380,** 1520–1529 (2012).
3. Keating, M. T. & Sanguinetti, M. C. Molecular and cellular mechanisms of cardiac arrhythmias. *Cell* **104,** 569–580 (Feb. 2001).
4. Fishman, G. I. *et al. Sudden cardiac death prediction and prevention: report from a National Heart, Lung, and Blood Institute and Heart Rhythm Society Workshop.* in *Circulation* (Lippincott Williams & Wilkins, Nov. 2010), 2335–2348.
5. Roden, D. M. Long-QT syndrome. *N Engl J Med* **358,** 169–176 (2008).
6. Giudicessi, J. R. & Ackerman, M. J. Potassium-channel mutations and cardiac arrhythmias—diagnosis and therapy. *Nat Rev Cardiol* **9,** 319–332 (Jan. 2012).
7. Crotti, L., Celano, G., Dagradi, F. & Schwartz, P. J. Congenital long QT syndrome. *Orphanet J Rare Dis* **3,** 18 (2008).
8. Kallergis, E. M., Goudis, C. A., Simantirakis, E. N., Kochiadakis, G. E. & Vardas, P. E. Mechanisms, Risk Factors, and Management of Acquired Long QT Syndrome: A Comprehensive Review. *The Scientific World Journal* **2012,** 1–8 (2012).
9. Wilde, A. & Bezzina, C. R. Genetics of cardiac arrhythmias. *Heart* **91,** 1352–1358 (2005).
10. Vitali, S. H. *et al.* The Sugen 5416/hypoxia mouse model of pulmonary hypertension revisited: long-term follow-up. *Pulmonary Circulation,* 000–000 (Oct. 2014).

11. Jervell, A. & Lange-Nielsen, F. Congenital deaf-mutism, functional heart disease with prolongation of the Q-T interval, and sudden death. *American Heart Journal* **54,** 59–68 (July 1957).

12. Schwartz, P. J., Crotti, L. & Insolia, R. Long-QT syndrome: from genetics to management. *Circulation: Arrhythmia and Electrophysiology* **5,** 868–877 (Aug. 2012).

13. Kapplinger, J. D. *et al.* Spectrum and prevalence of mutations from the first 2,500 consecutive unrelated patients referred for the FAMILION long QT syndrome genetic test. *Heart Rhythm* **6,** 1297–1303 (Sept. 2009).

14. Medeiros-Domingo, A., Iturralde-Torres, P. & Ackerman, M. J. Clinical and Genetic Characteristics of Long QT Syndrome. *Rev Esp Cardiol (Engl Ed)* **60,** 739–752 (2007).

15. Schwartz, P. J. *et al.* Prevalence of the congenital long-QT syndrome. *Circulation* **120,** 1761–1767 (Nov. 2009).

16. Crotti, L. *et al.* Common KCNH2 Polymorphism (K897T) as a genetic modifier of congenital long QT syndrome. *HRTHM* **2,** S111 (Jan. 2005).

17. Crotti, L *et al.* NOS1AP is a genetic modifier of the long-QT syndrome. - PubMed - NCBI. *Circulation* **120,** 1657–1663 (Oct. 2009).

18. Ackerman, M. J. *et al.* Ethnic differences in cardiac potassium channel variants: implications for genetic susceptibility to sudden cardiac death and genetic testing for congenital long QT syndrome. *Mayo Clin. Proc.* **78,** 1479–1487 (Dec. 2003).

19. Earle, N. *et al.* Single nucleotide polymorphisms in arrhythmia genes modify the risk of cardiac events and sudden death in long QT syndrome. *Heart Rhythm* **11,** 76–82 (Jan. 2014).

20. De Villiers, C. P. *et al.* AKAP9 Is a Genetic Modifier of Congenital Long-QT Syndrome Type 1. *Circ Cardiovasc Genet* **7,** 599–606 (Oct. 2014).

21. Giudicessi, J. R. & Ackerman, M. J. Genotype- and Phenotype-Guided Management of Congenital Long QT Syndrome. *Current Problems in Cardiology* **38,** 417–455 (Oct. 2013).

22. Sanguinetti, M. C. & Tristani-Firouzi, M. hERG potassium channels and cardiac arrhythmia. *Nature* **440,** 463–469 (Mar. 2006).

23. Fernandez, D., Ghanta, A., Kauffman, G. W. & Sanguinetti, M. C. Physicochemical features of the HERG channel drug binding site. *Journal of Biological Chemistry* **279,** 10120–10127 (Mar. 2004).

24. Roden, D. M. Drug-induced prolongation of the QT interval. *N Engl J Med* **350,** 1013–1022 (Mar. 2004).

25. Dupuis, B. in *Drug Evaluation in Angina Pectoris* 255–258 (Springer US, London, Jan. 1994).

26. Redfern, W. S. *et al.* Relationships between preclinical cardiac electrophysiology, clinical QT interval prolongation and torsade de pointes for a broad range of drugs: evidence for a provisional safety margin in drug development. *Cardiovascular Research* **58,** 32–45 (Apr. 2003).

27. Gussak, I., Litwin, J., Kleiman, R., Grisanti, S. & Morganroth, J. Drug-induced cardiac toxicity: emphasizing the role of electrocardiography in clinical research and drug development. *J Electrocardiol* **37,** 19–24 (Jan. 2004).

28. Liang, P. *et al.* Drug screening using a library of human induced pluripotent stem cell-derived cardiomyocytes reveals disease-specific patterns of cardiotoxicity. *Circulation* **127,** 1677–1691 (Apr. 2013).

29. Makkar, R. R., Fromm, B. S., Steinman, R. T., Meissner, M. D. & Lehmann, M. H. Female gender as a risk factor for torsades de pointes associated with cardiovascular drugs. *JAMA* **270,** 2590–2597 (Dec. 1993).

30. Rautaharju, P. M. *et al.* Sex differences in the evolution of the electrocardiographic QT interval with age. *Can J Cardiol* **8,** 690–695 (Sept. 1992).

31. Arya, A. Gender-related differences in ventricular repolarization: beyond gonadal steroids. *J Cardiovasc Electrophysiol* **16,** 525–527 (May 2005).

32. Yang, T, Snyders, D. J. & Roden, D. M. Rapid inactivation determines the rectification and [K+]o dependence of the rapid component of the delayed rectifier K+ current in cardiac cells. *Circulation Research* **80,** 782–789 (June 1997).

33. Yang, T & Roden, D. M. Extracellular potassium modulation of drug block of IKr. Implications for torsade de pointes and reverse use-dependence. *Circulation* **93,** 407–411 (Feb. 1996).

34. Rocchetti, M *et al.* Rate dependency of beta-adrenergic modulation of repolarizing currents in the guinea-pig ventricle. *J. Physiol. (Lond.)* **574,** 183–193 (July 2006).

35. Namboodiri, N. Bradycardia-induced Torsade de Pointes - An arrhythmia Less Understood. *Indian Pacing Electrophysiol J* **10,** 435–438 (2010).

36. Kléber, A. G. & Rudy, Y. Basic mechanisms of cardiac impulse propagation and associated arrhythmias. *Physiological Reviews* **84,** 431–488 (Apr. 2004).

37. Hoffman, B. F. & Rosen, M. R. Cellular mechanisms for cardiac arrhythmias. *Circulation Research* **49,** 1–15 (July 1981).

38. Weiss, J. N., Garfinkel, A., Karagueuzian, H. S., Chen, P.-S. & Qu, Z. Early afterdepolarizations and cardiac arrhythmias. *Heart Rhythm* **7,** 1891–1899 (Dec. 2010).

39. Cranefield, P. F. Action potentials, afterpotentials, and arrhythmias. *Circulation Research* **41,** 415–423 (Oct. 1977).

40. Venetucci, L. A., Trafford, A. W., O'Neill, S. C. & Eisner, D. A. Na/Ca exchange: regulator of intracellular calcium and source of arrhythmias in the heart. *Annals of the New York Academy of Sciences* **1099,** 315–325 (Mar. 2007).

41. Schwartz, P. J. Idiopathic long QT syndrome: Progress and questions. *American Heart Journal* **109,** 399–411 (Feb. 1985).

42. Schwartz, P. J., Moss, A. J., Vincent, G. M. & Crampton, R. S. Diagnostic criteria for the long QT syndrome. An update. *Circulation* **88,** 782–784 (Aug. 1993).

43. Schwartz, P. J. The congenital long QT syndromes from genotype to phenotype: clinical implications. *J. Intern. Med.* **259,** 39–47 (Jan. 2006).

44. Schwartz, P. J. & Ackerman, M. J. The long QT syndrome: a transatlantic clinical approach to diagnosis and therapy. *European Heart Journal* **34,** 3109–3116 (Oct. 2013).

45. Moss, A. J. *et al.* ECG T-wave patterns in genetically distinct forms of the hereditary long QT syndrome. *Circulation* **92,** 2929–2934 (Nov. 1995).

46. Priori, S. G. & Napolitano, C. Meandering pathway leading from genotyping to personalized management of long-QT syndrome. *Circulation* **125,** 1961–1963 (Apr. 2012).

47. Schwartz, P. J. *et al.* Genotype-phenotype correlation in the long-QT syndrome: gene-specific triggers for life-threatening arrhythmias. *Circulation* **103,** 89–95 (Jan. 2001).

48. Ackerman, M. J., Tester, D. J. & Porter, C. J. Swimming, a gene-specific arrhythmogenic trigger for inherited long QT syndrome. *Mayo Clin. Proc.* **74,** 1088–1094 (Nov. 1999).

49. Wilde, A. A. *et al.* Auditory stimuli as a trigger for arrhythmic events differentiate HERG-related (LQTS2) patients from KVLQT1-related patients (LQTS1). *JAC* **33,** 327–332 (Feb. 1999).

50. Moss, A. J. *et al.* Clinical aspects of type-1 long-QT syndrome by location, coding type, and biophysical function of mutations involving the KCNQ1 gene. *Circulation* **115,** 2481–2489 (May 2007).

51. Moss, A. J. *et al.* Increased risk of arrhythmic events in long-QT syndrome with mutations in the pore region of the human ether-a-go-go-related gene potassium channel. *Circulation* **105,** 794–799 (Feb. 2002).

52. Priori, S. G., Napolitano, C & Schwartz, P. J. Low penetrance in the long-QT syndrome: clinical impact. *Circulation* **99,** 529–533 (Feb. 1999).

53. Wilde, A. A. & Roden, D. M. Predicting the long-QT genotype from clinical data: from sense to science. *Circulation* **102,** 2796–2798 (Dec. 2000).

54. Schwartz, P. J. Practical issues in the management of the long QT syndrome: focus on diagnosis and therapy. *Swiss Med Wkly* **143,** w13843 (2013).

55. Vincent, G. M. *et al.* High efficacy of beta-blockers in long-QT syndrome type 1: contribution of noncompliance and QT-prolonging drugs to the occurrence of beta-blocker treatment "failures". *Circulation* **119,** 215–221 (Jan. 2009).

56. Priori, S. G. *et al.* Association of long QT syndrome loci and cardiac events among patients treated with beta-blockers. *JAMA* **292,** 1341–1344 (Sept. 2004).

57. Schwartz, P. J. *et al.* Left Cardiac Sympathetic Denervation in the Therapy of Congenital Long Qt Syndrome - a Worldwide Report. *Circulation* **84,** 503–511 (Aug. 1991).

58. Schwartz, P. J. *et al.* Who are the long-QT syndrome patients who receive an implantable cardioverter-defibrillator and what happens to them?: data from the European Long-QT Syndrome Implantable Cardioverter-Defibrillator (LQTS ICD) Registry. *Circulation* **122,** 1272–1282 (Sept. 2010).

59. Blazeski, A. *et al.* Electrophysiological and contractile function of cardiomyocytes derived from human embryonic stem cells. *Prog. Biophys. Mol. Biol.* **110,** 178–195 (Oct. 2012).

60. Zhang, J. *et al.* Functional cardiomyocytes derived from human induced pluripotent stem cells. *Circulation Research* **104,** e30–41 (Feb. 2009).

61. Cheung, C., Bernardo, A. S., Trotter, M. W. B., Pedersen, R. A. & Sinha, S. Generation of human vascular smooth muscle subtypes provides insight into embryological origin–dependent disease susceptibility. *Nat. Biotechnol.* **30,** 165–173 (Jan. 2012).

62. Mummery, C. *et al.* Differentiation of human embryonic stem cells to cardiomyocytes: role of coculture with visceral endoderm-like cells. *Circulation* **107,** 2733–2740 (June 2003).

63. Laflamme, M. A. *et al.* Cardiomyocytes derived from human embryonic stem cells in pro-survival factors enhance function of infarcted rat hearts. *Nat. Biotechnol.* **25,** 1015–1024 (Aug. 2007).

64. Yang, L. *et al.* Human cardiovascular progenitor cells develop from a KDR+ embryonic-stem-cell-derived population. *Nature* **453,** 524–528 (Apr. 2008).

65. Loi, P. *et al.* Sheep: The First Large Animal Model in Nuclear Transfer Research. *Cell Reprogram* **15,** 367–373 (2013).

66. Bellin, M., Marchetto, M. C., Gage, F. H. & Mummery, C. L. Induced pluripotent stem cells: the new patient? *Nat Rev Mol Cell Biol* **13,** 713–726 (Nov. 2012).

67. Matsa, E., Burridge, P. W. & Wu, J. C. Human stem cells for modeling heart disease and for drug discovery. *Sci Transl Med* **6,** 239ps6–239ps6 (June 2014).

68. Kim, K *et al.* Epigenetic memory in induced pluripotent stem cells. *Nature* **467,** 285–290 (Sept. 2010).

69. Lister, R. *et al.* Hotspots of aberrant epigenomic reprogramming in human induced pluripotent stem cells. *Nature* **471,** 68–73 (Feb. 2011).

70. Takahashi, K. *et al.* Induction of Pluripotent Stem Cells from Adult Human Fibroblasts by Defined Factors. *Cell* **131,** 861–872 (Nov. 2007).

71. Yu, J. *et al.* Induced pluripotent stem cell lines derived from human somatic cells. *Science* **318,** 1917–1920 (Dec. 2007).

72. Yamashita, M. & Emerman, M. Retroviral infection of non-dividing cells: old and new perspectives. *Virology* **344,** 88–93 (Jan. 2006).

Chapter 2

CALM1^{F142L} mutation

2.1 Acronyms

C$_m$	membrane capacitance
DC	dynamic clamp
E$_{diast}$	diastolic potential
I$_{K1}$	inward rectifier K^+ current
4-AP	4-aminopyridine
APD	AP duration
FPD	field potential duration
APD$_{90}$	APD at 90% of repolarization phase
APD$_{50}$	APD at 50% of repolarization phase
CDI	Ca^{2+}-calmodulin dependent inactivation
r$_{100}$	I_{CaL} remaining 100 ms after peak
r$_{300}$	I_{CaL} remaining 300 ms after peak
I$_{BaL}$	L-type Ba^{2+} current
MEA	MultiElectrode Array
EB	embryoid bodies
ISO	isoprenaline

CaM	calmodulin
$\mathbf{G}_{max}$	maximal conductance
$\mathbf{E}_{rev}$	reversal potential

2.2 Introduction

Calmodulin (CaM) is a small ubiquitous Ca^{2+} binding protein present in all eukaryotic cells [1] which exerts its modulatory role depending on intracellular Ca^{2+} concentration changes [2]. It is encoded by 3 genes: CALM1, CALM2, CALM3 which generate an identical 148 aminoacids protein. Four Ca^{2+}-binding sites with EF-hand structure are present in two lobes at the N- and C- terminus of the protein. Ca^{2+} ions binding is cooperative and induces conformational changes in the lobes from the *closed* state, defined apo-CaM, to the *open* state (Ca_2- or Ca_4-CaM). This allows CaM binding to a large number of biological targets [1]. CaM regulates diverse cellular functions like myocytes contraction [3], immunological response [4] and neuronal excitability [5]. Furthermore, CaM mutations have been linked with an heterogeneous spectrum of pathologies as heart failure [6], Alzheimer's disease [7], Parkinson's disease [8] and muscular dystrophies [9]. In the heart, CaM mutations have been recently found associated with LQTS phenotype, recurring cardiac arrest in infants [10], arrhythmia susceptibility [11] and SCD [12]. The localization of these mutations is restricted to key residues belonging to or flanking the Ca^{2+}-binding domains (table 2.1).

Mutant CaM evidenced in vitro a strongly altered Ca^{2+}-binding affinity, which is hypothesized to be the primary cause of pathological manifestations. Since all the three CALM genes encode for an identical protein [12], the extremely severe phenotype observed in vitro seem to be overestimated for an heterozygous mutation which can be compensated by other five wild type analogues.

Gene	Mutation	Phenotype
CALM1	p.N53I[12]	CPVT
	p.N97S[12]	CPVT
	p.D130G[10]	LQTS
	p.F142L[10]	LQTS
CALM2	p.D96V[10]	LQTS
	p.N98S[11]	LQTS
	p.N98I[11]	LQTS
	p.D132E[11]	CPVT
	p.D134H[11]	LQTS
	p.Q136P[11]	CPVT

Table 2.1: Recent CaM mutations associated with cardiac phenotype [10][12]. CPVT = Catecholaminergic Polymorphic Ventricular Tachycardia. In orange is highlighted the mutation characterized in this study.

Here we focus the attention on the heterozygous F142L mutation in CALM1 gene, which evidenced a strong increase in K_d for binding of Ca^{2+} ions to CaM C-terminal domain by more than five folds [10]. Recent studies in heterologous systems [13][14] or mouse models [15] confirmed the disrupted Ca^{2+}-binding activity of over-expressed mutated CaM; furthermore, they demonstrated that I_{CaL} is the primary cell function altered by the mutation. However, the extremely severe phenotype observed in vitro was not perfectly consistent with clinical data and all the experiments were performed by over-expressing mutant CaM leading to potentially deceptive results since the lack of compensatory activity from the products of other CALM genes, of which CALM1 is described as the least transcribed [10]. Moreover, the mechanism explaining the high arrhythmia susceptibility and the severe phenotype of this patient is still unknown. Two main hypothesis can then be made: arrhythmogenic risk may derive from 1) Ca^{2+}-handling abnormalities or 2) electrical instability. Using patient-specific hiPSC-CMs, we studied the functional consequences of CaM F142L mutation on I_{CaL} biophysics and intracellular Ca^{2+} dynamics in isolated cells and EB. Then, we evaluated AP in native condition and in the pres-

ence of computational-simulated inward rectifier K^+ current (I_{K1}) injected with dynamic clamp (DC). Finally, field potential duration (FPD) and its isoprenaline (ISO) sensitivity were assessed with 256-electrodes MEA. We found that F142L mutation strongly impaired Ca^{2+}-calmodulin dependent inactivation (CDI) of I_{CaL}, increased window current, significantly prolonged APD and FPD, increased Ca^{2+}-transient amplitude and fractional release from the SR. Moreover, a low level of AP adaptation to high frequency was evidenced in F142L cells, pointing this as a likely arrhythmogenic mechanism for the mutation.

2.3 Methods

2.3.1 Patients

Patient with F142L mutation was a 14-year old Caucasian male from Italy, who was adopted at age 8. Since birth, he was under β-blocker therapy (propranolol) and experienced multiple episodes of loss of consciousness and seizures. In addition, he had severe cognitive dysfunctions and was treated for epilepsy with valproate and carbamazepine. At age 10, a clinical evaluation evidenced a strongly prolonged QT_c (>600 ms) associated with T-wave alternans and ventricular tachycardia. Echocardiography did not reveal structural and contractile abnormalities. Screening for classical LQTS genes did not find mutation in *KCNQ1*, *KCNH2*, *SCN5A*, *KCNE1* and *KCNE2*. Nocturnal bradycardia (32 beats per minute) limited the propranolol dosage escalation. Mexiletine reduced T-wave alternans and suppressed ventricular arrhythmias but it was not included in the therapy since it failed to shorten QT_c. At age 11, LCSD was performed and an ICD was implanted following recurrent episodes of ventricular fibrillation [10].

2.3.2 hiPSC-CMs generation

Since F142L patient was adopted, relatives' samples were unavailable. For this reason, we decided to use two different sources of controls iPS: CTR one, clone 6 (C6), fibroblasts were obtained from an healthy caucasian woman, while CTR two, human adult keratinocytes (HAK), clone 8, were obtained from an afro-american male donor. Two clones from F142L patient were used for functional measurements to exclude clone-specific effects and improve the reliability of the results. hiPSC-CMs were generated as previously described [16]. Briefly, skin fibroblast (CTR C6, F142L c1, F142L c11) or keratinocytes (CTR HAK) were collected from healthy donors and patients via biopsy. Samples were minced into 2 mm pieces and cultured into Petri dishes with Quantum 333 medium. Fibroblasts migrating out of the explants were separated and cultured before retroviral infection with human transcription factors OCT3/4, SOX2, KLF4 and c-MYC [17]. After 6 days, cells were co-cultured over a murine embryonic fibroblasts (MEF) feeder layer and maintained, until pluripotency was reached, in human embryonic stem cell medium containing: DMEM F12, supplemented with 20% knockout serum replacement (KSR), L-glutamine (2 mM), non-essential aminoacids (NEAA, 0.1 mM) β-mercaptoethanol (0.1 mM), penicillin / streptomycin (1:100) and basic fibroblast growth factor (b-FGF, 10 ng/mL). After 3 to 4 weeks, colonies were manually detached from MEF using phosphate buffered saline (PBS) containing trypsin (2.5 mg/mL), collagenase IV (1 mg/mL) and $CaCl_2$ (1 mM). Spontaneous differentiation was then induced by replacing the standard medium with: DMEM F12 supplemented with 20% fetal bovine serum (FBS), L-glutamine (2 mM), NEAA (0.1 mM), β-mercaptoethanol (0.1 mM) and penicillin/streptomycin (1:100). Cardiac differentiation was improved by adding ascorbic acid (50 μg/mL) on day 7. At day 20-30 of differentiation, EB were manually

dissected and plated on fibronectin-coated dishes. These explants were maintained in the differentiation medium with 2% FBS. Dissociation of isolated hiPSC-CMs from EB, for electrophysiological and immunofluorescence analyses, were performed with type II collagenase at 37 °C under shaking. EB and isolated hiPSC-CMs were used for experiments at 70-90 days of differentiation.

2.3.3 Patch Clamp

2.3.3.1 I_{CaL} measurements

I_{CaL} was isolated with Na^+- and K^+-free solution containing (mM): 140 tetraethylammonium chloride (TEACl), 5 $CaCl_2$, 5 HEPES, 1 $MgCl_2$, 10 D-glucose. 2 mM 4-aminopyridine (4-AP) was added to prevent contamination from transient outward K^+ current. pH was adjusted to 7.4 with HCl. Additionally, 10 μM TTX was used to avoid potential contamination of Ca^{2+} ions flowing through Na^+ channels. For L-type Ba^{2+} current (I_{BaL}) measurements, Ca^{2+} was replaced with an equal concentration of Ba^{2+}. Intracellular solution contained (mM): 115 CsCl, 20 TEACl, 0.5 $MgCl_2$, 10 EGTA CsOH, 5 HEPES CsOH, 5 ATP Mg^{2+} salt, 5 phosphocreatine, 0.4 GTP Tris salt; pH was adjusted to 7.2 with CsOH. To prevent fast current rundown, I_{CaL} measurements were performed at room temperature. I_{CaL} remaining 100 ms after peak (r_{100}) and I_{CaL} remaining 300 ms after peak (r_{300}) were evaluated as the current remaining respectively 100 ms and 300 ms after the peak of I_{CaL} or I_{BaL}. Data were then divided by the respective current peak value. In matched cells, I_{BaL} r_{100} values were subtracted to I_{CaL} ones to derive the contribution of CDI. Activation and inactivation curves were fitted with a Boltzmann equation to extract key parameters as voltage of half activation/inactivation ($V_{0.5}$), slope (k), maximal conductance (g_{max}) and ratio between minimal conductance (g_{min}) and g_{max}. Window

I_{CaL} was quantified by analyzing its area, the peak value and the maximum probability (P_{max}). Series resistance was compensated to maintain the error on the imposed voltage under 3.5 mV. Signals were acquired with a MultiClamp 200B amplifier (Molecular Devices), connected to a Digidata 1440A (Molecular Devices) and filtered with a Bessel at 2 kHz via pClamp 10.4 (Molecular Devices).

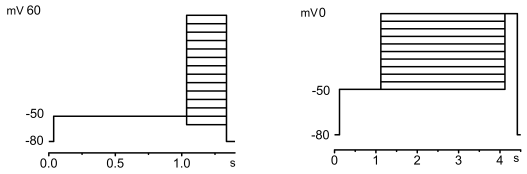

Figure 2.1: *Voltage clamp protocols: Left:* I_{CaL} steady state activation protocol. *Right:* I_{CaL} steady state inactivation protocol.

2.3.3.2 Intracellular Ca^{2+} measurements

Intracellular Ca^{2+} measurements were performed by patch clamp in epifluorescence. Considering the heterogeneous nature of iPS, which was particularly evident for diastolic potential (E_{diast}), we decided to use a voltage clamp protocol to increase the uniformity of the measurements. Tyrode's solution containing (mM): 140 NaCl, 4 KCl, 2 $CaCl_2$, 1.2 $MgCl_2$, 5 HEPES and 11 D-glucose, adjusted to pH 7.4 with NaOH. 2 mM 4-AP and 1 mM $BaCl_2$ were added to prevent K^+ currents contamination. 10 mM caffeine was dissolved in Ca^{2+}-free Tyrode's solution. Cells were incubated 1 hour with 10 μM Fluo-4AM at room temperature and then washed with Tyrode's for 10 minutes to allow de-esterification. Fluo4 emission was collected through a 535 nm band pass filter, converted to voltage, low-pass filtered (200 Hz) and digitized at 2 kHz after further low-pass digital filtering (FFT, 100 Hz). Fluorescence decay after caffeine application (empty SR) was used as reference (F_0) for signal normalization (F/F_0) after subtraction of background lumi-

nescence. Pipette solution contained (mM): 110 K-aspartate, 23 KCl, 3 $MgCl_2$, 0.2 $CaCl_2$, 5 HEPES-KOH, 0.5 EGTA-KOH, 5 ATP Na^+-salt, 5 phosphocreatine, 0.4 GTP Na^+ salt; pH was adjusted to 7.3 with KOH. Measurements were performed at 36 °C. Protocols for voltage clamp experiments are indicated in figure 2.1.

2.3.3.3 Action potentials rate-dependency

hiPSC-CMs have low expression of I_{K1}, with a consequent depolarized E_{diast} and the presence of automatic activity in ventricular-like cells. This leads to an incomplete channel recruiting, generating abnormal and non physiological AP. We addressed this issue with a DC approach [18]: a human I_{K1} numerical model, derived from the Rudy-O'Hara model [19], was injected into hiPSC-CMs. To achieve a physiological diastolic potential, reversal potential (E_{rev}) was set to -80 mV. Furthermore, maximal conductance (G_{max}) required a 10 fold increase (1.9 nS/μF) to match the I_{K1} density of adult myocytes [20]. The model was injected using the Real-Time eXperiment Interface (RTXI, [21]) running on Ubuntu 10.04 LTS, paired with an A/D converter (BNC-2120, National Instruments, Austin, TX, USA). AP experiments were performed at four different frequencies (0.5 Hz, 1 Hz, 2 Hz, 3 Hz) to investigate the rate-dependence of AP in both native and DC conditions. Tyrode's solution at 36 °C with a pipette solution containing (mM): 110 K-aspartate, 23 KCl, 3 $MgCl_2$, 5 HEPES-KOH, 0.5 EGTA-KOH, 5 ATP Na^+-salt, 5 phosphocreatine, 0.4 GTP Na^+ salt; pH was adjusted to 7.3 with KOH.

2.3.4 Contraction

EBs contractions pattern were recorded on spontaneously beating clusters with an edge detection system connected to Multiclamp 200B Amplifier and Digidata 1440A.

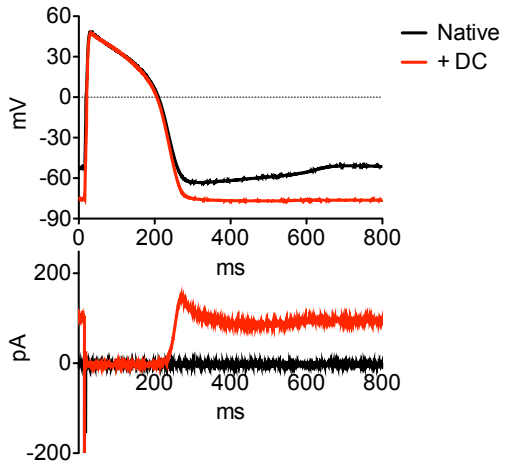

Figure 2.2: Action potentials recorded from an isolated hiPSC-CMs by patch clamp. Comparison between native AP (black) and AP obtained by injecting a computational model of I_{K1} in real time (+DC, red).

2.3.5 MultiElectrode Array (MEA)

Field Potentials were recorded from spontaneously beating EB with a 256-electrode MEA (Multi Channel Systems). MEA chambers were coated with Matrigel for 1h before seeding the EB. EB2 medium containing 2% FBS and supplemented with 200 mM L-glutamine, 1:100 NEAA, 1:100 Penicillin /Streptomycin was used for the recordings. isoprenaline (ISO) was used at 4 different concentrations (μM): 50, 300, 600, 1600. All substances were added with a pipette in volumes of 5 μL. A 100 fold dilution was used considering a MEA chamber volume of 500 μL. Steady state was reached within 5 minutes of recording. Data analysis was performed with MC Rack, MC Data Tool (Multi Channel Systems) and pClamp suite (Molecular Devices). QT intervals were assumed here as representative of FPD and obtained from the first peak of depolarization, indicating the phase 0 of the AP, to the last repolarizing peak, correspondent to the AP repolarization [22]. QT_c intervals were calculated with standard Bazett's (QTc_B, $\frac{QT}{\sqrt{RR}}$) and

Fridericia's (QTc_F, $\frac{QT}{\sqrt[3]{RR}}$) corrections.

2.3.6 Statistics

Student's t-test or ANOVA for paired or unpaired measurements were applied as appropriate to test for significance between means. A two-tailed Mann-Whitney test was used for the analysis of non-parametric distrubutions. A two-tailed Wilcox matched pairs test was used for the analysis of paired observations. Post hoc comparison between individual means was performed by BonferroniÕs or DunnÕs multiple comparison tests. Data in bars are expressed and plotted as the mean ± standard error of the mean. Fisher's exact test was used for the analysis of AP alternans. Statistical significance was defined as $p < 0.05$ (n.s., not significant). The sample size for each experiment is specified in the respective figure legend. All the analyses were performed with GraphPad Prism v5.0c for Mac.

2.4 Results

2.4.1 Cellular parameters

The average membrane capacitance (C_m) was equal in all group: 31.7 ± 2.7 pF for CTR C6, 38.9 ± 5.9 pF for CTR HAK, 45.3 ± 3.4 pF for F142L c1, 32.3 ± 2.7 pF for F142L c11. The vast majority of cells evidenced a ventricular-like phenotype, while only a few atrial or nodal-like were observed. Details on cell number and experimental groups are indicated in figure legends.

2.4.2 Clone consistency

Two sources of CTR were used and compared since no data were available on F142L relatives as a consequence of an early adoption.

CTR C6 and HAK were firstly compared in voltage clamp condition. CTR HAK evidenced an increased I_{CaL} density compared to CTR C6 (figure 2.3). Differences emerged from the comparison of steady state activation and inactivation kinetics of I_{CaL} (figure 2.3); I_{CaL} window current was equal in both groups (table 2.2). CDI parameters, as r_{100} and 300 ms after the peak (r_{300}), were identical between the two groups, indicating that this property is highly consistent among these lines and could be used as reference for CTR (figures 2.5 and 2.4).

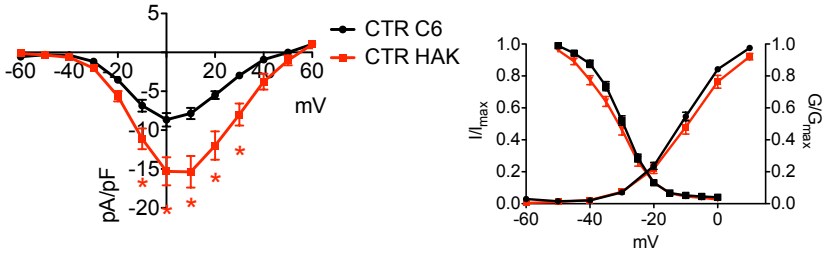

Figure 2.3: *Biophysical parameters of I_{CaL} Left:* Average traces of I_{CaL} from CTR lines C6 and HAK. *Right:* Average activation and inactivation curves for CTR clones C6 and HAK. n = 11, 11. $*$ = p <0.05 vs CTR.

	CTR	
	C6	**HAK**
	Activation	
$V_{0.5}$ (mV)	-11.3 ± 0.78	-8.3 ± 1.8$*$
k (mV)	6.7 ± 0.27	7.9 ± 0.35$*$
g_{max} (nS/pF)	0.22 ± 0.03	0.4 ± 0.05$*$
	Inactivation	
$V_{0.5}$ (mV)	-30.2 ± 0.62	-31.7 ± 0.9
k (mV)	4.8 ± 0.29	6.1 ± 0.3$*$
G_{min}/G_{max}	0.03 ± 0.005	0.02 ± 0.006
	Window I_{CaL}	
Area (a.u.)	2.90 ± 0.3	3.0 ± 0.5
Peak (mV)	-21.87 ± 0.8	-21.89 ± 1.4
Pmax	0.17 ± 0.01	0.18 ± 0.01

Table 2.2: Average parameters obtained for CTR C6 and HAK. $*$ = p <0.05 vs CTR C6. n >11, 6.

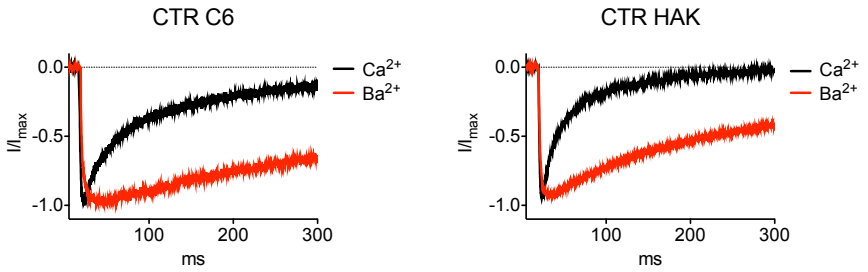

Figure 2.4: Examples of I_{CaL} (black) and I_{BaL} (red) recorded in CTR C6 and CTR HAK clones. Traces were normalized to current peak. Identical CDI was observed for both CTR group, with a fast I_{CaL} inactivation after 300 ms.

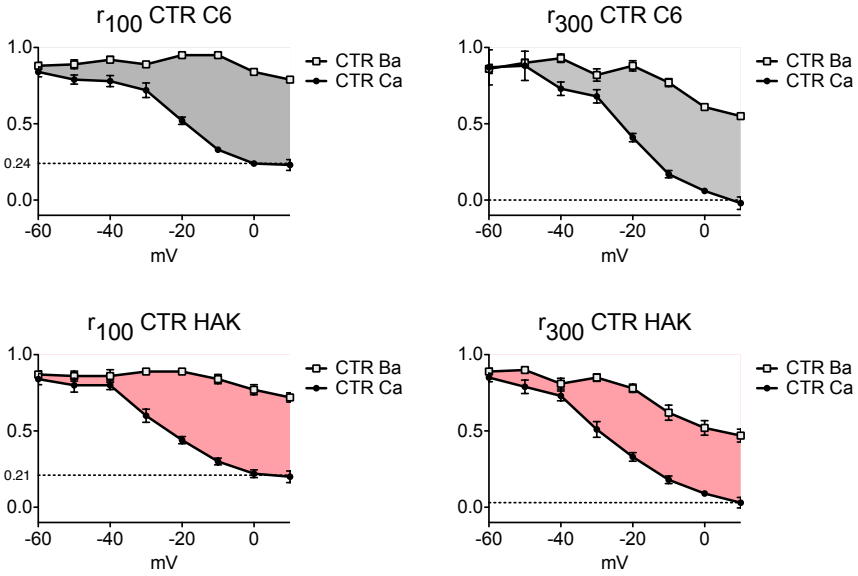

Figure 2.5: *CDI analysis*: r_{100} and r_{300} parameters for CTR C6 (dark grey) and HAK (red). CDI is defined as the colored area between I_{CaL} and I_{BaL}. No differences were evidenced in these parameters, confirming equal structure and function for $Ca_v1.2$. n = 10, 12.

Current clamp measurements confirmed the clone consistency between CTR C6 and HAK on APD at 90% of repolarization phase (APD_{90}) at all pacing frequencies in both native and DC conditions (figure 2.6). Average results are listed in tables 2.3 and 2.4.

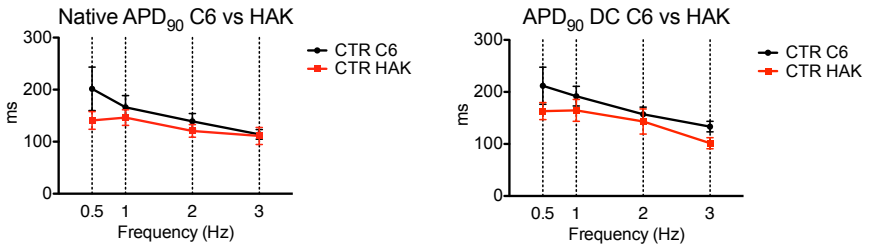

Figure 2.6: Comparison of native (*left*) and DC (*right*) APD_{90} between CTR C6 and CTR HAK. n at each frequency = 9, 13, 11, 8 for C6; 7, 9, 7, 6 for HAK.

Given the almost complete clone consistency between two profoundly different sources of controls, we decided to focus the following comparisons on CTR C6 since using a reference with the same ethnicity could minimize random differences in the comparisons. A complete uniformity was observed also for F142L clones, thus we decided to merge the data since they were derived from the same cell source.

Parameter	CTR C6				CTR HAK			
	Frequency (Hz)							
	0.5	1	2	3	0.5	1	2	3
E_{diast} (mV)	-49.5 ± 3.4	-47.4 ± 2.7	-48.3 ± 3.0	-46.8 ± 3.7	-46.7 ± 3.3	-47.1 ± 3.2	-53.9 ± 3.2	-58.3 ± 3.9
APD_{50} (ms)	145.2 ± 36.4	113.3 ± 18.9	84.9 ± 11.9	62.9 ± 7.4	105.8 ± 16.8	98.6 ± 13.6	75.9 ± 9.0	70.2 ± 12.7
APD_{90} (ms)	201.6 ± 41.8	166.1 ± 22.5	139.0 ± 15.0	114.1 ± 9.3	140.9 ± 16.9	146.4 ± 14.9	120.7 ± 12.1	111.0 ± 16.5
APD_{50}/APD_{90}	0.64 ± 0.06	0.63 ± 0.05	0.59 ± 0.04	0.55 ± 0.04	0.78 ± 0.03	0.71 ± 0.02	0.65 ± 0.02	0.57 ± 0.03
peak amplitude (mV)	40.3 ± 3.9	39.0 ± 3.4	37.8 ± 2.8	29.2 ± 4.3	44.6 ± 1.9	37.1 ± 4	34.1 ± 5.0	37.4 ± 5.7

Table 2.3: Native AP parameters for CTR C6 and CTR HAK at 4 pacing frequencies.

Parameter	CTR C6				CTR HAK			
	Frequency (Hz)							
	0.5	1	2	3	0.5	1	2	3
E_{diast} (mV)	-75.3 ± 1.1	-75.1 ± 1.4	-76.4 ± 0.7	-76.6 ± 0.5	-74.6 ± 0.6	-75.6 ± 1.0	-76.9 ± 0.7	-77.7 ± 0.6
APD_{50} (ms)	159.0 ± 32.2	133.0 ± 18.6	95.1 ± 12.2	75.8 ± 10.1	114.7 ± 13.9	101.2 ± 13.7	84.4 ± 8.0	67.44 ± 8.8
APD_{90} (ms)	211.9 ± 35.7	191.9 ± 18.9	157.0 ± 13.9	133.5 ± 10.1	163.2 ± 16.4	164.7 ± 21.1	143.4 ± 24.1	101.55 ± 10.6
APD_{50}/APD_{90}	0.70 ± 0.07	0.65 ± 0.06	0.59 ± 0.05	0.57 ± 0.06	0.70 ± 0.04	0.7 ± 0.04	0.69 ± 0.02	0.66 ± 0.03
peak amplitude (mV)	43.6 ± 2.1	43.7 ± 1.7	41.8 ± 1.7	38.0 ± 2.7	40.5 ± 1.5	39.4 ± 2.3	39.3 ± 4.1	40.2 ± 4.2
I_{K1} peak (pA/pF)	-2.49 ± 0.03	-2.48 ± 0.01	-2.47 ± 0.02	-2.47 ± 0.02	-2.45 ± 0.02	-2.8 ± 0.2	-2.26 ± 0.2	-2.46 ± 0.2
I_{K1} diastolic (pA/pF)	-1.69 ± 0.2	- 1.50 ± 0.2	-1.45 ± 0.2	-1.45 ± 0.2	-2.01 ± 0.13	-1.52 ± 0.2	-1.22 ± 0.2	-1.02 ± 0.17

Table 2.4: DC AP parameters for CTR C6 and CTR HAK clones at 4 pacing frequencies.

2.4.3 F142L mutation

2.4.3.1 Calcium current

Since CaM targets primarily the L-type Ca^{2+} channel, we investigated potential differences in I_{CaL} biophysical properties. No differences in I_{CaL} densities were evidences between CTR C6 and two F142L clones (figure 2.7). Steady-state activation parameters were identical among the three experimental groups. However, both F142L clones evidenced a decreased and incomplete steady-state inactivation. Furthermore, we observed a significantly increased window current (figure 2.8). Parameters from the quantitative analysis are summarized in table 2.5.

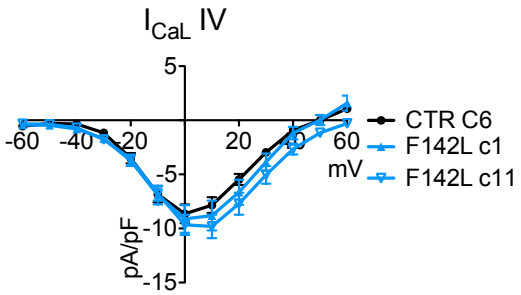

Figure 2.7: No differences were evidenced in I_{CaL} densities between CTR C6 and F142L clones. n = 12.

The analysis of r_{100} and r_{300} indicated an identical and markedly decreased CDI similarly for both F142L clones (figure 2.9). In specific, 75% of I_{CaL} was inactivated in CTR 100 ms after peak at 0 mV, compared to 50% in F142L clones. Furthermore, 300 ms after peak, CTR showed a complete inactivation of I_{CaL} while F142L clones had 25% of the current still not inactivated (figure 2.10). CDI, obtained as subtraction between I_{CaL} and I_{BaL} (figure 2.11), is substantially reduced in F142L clones.

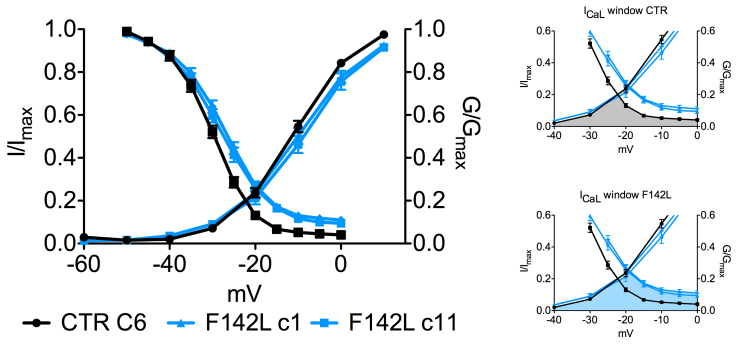

Figure 2.8: *Left:* Activation and inactivation curves for CTR C6 and F142L clones. Incomplete inactivation is present in both F142L clones. *Right:* Increased window current in F142L clones (blue) compared to CTR C6 (dark grey). Average data are presented in table 2.5. n >11, 12, 12.

	CTR	**F142L**	
	C6	**C1**	**C11**
		Activation	
$V_{0.5}$ (mV)	-11.3 ± 0.78	-9.9 ± 1.12	-8.9 ± 1.42
k (mV)	6.7 ± 0.27	7.7 ± 0.31∗	7.8 ± 0.35∗
g_{max} (nS/pF)	0.22 ± 0.03	0.25 ± 0.03	0.26 ± 0.05
		Inactivation	
$V_{0.5}$ (mV)	-30.2 ± 0.62	-28.0 ± 0.7∗	-28.5 ± 0.8∗
k (mV)	4.8 ± 0.29	5.5 ± 0.31∗	5.8 ± 0.15∗
G_{min}/G_{max}	0.03 ± 0.005	0.1 ± 0.01∗	0.08 ± 0.01∗
		Window I_{CaL}	
Area (a.u.)	2.90 ± 0.3	5.22 ± 0.4∗	4.84 ± 0.8∗
Peak (mV)	-21.87 ± 0.8	-17.81 ± 0.9∗	-19.21 ± 1.4
Pmax	0.17 ± 0.01	0.25 ± 0.008 ∗	0.24 ± 0.02∗

Table 2.5: Average parameters obtained for CTR C6 and both F142L clones. ∗ = p <0.05 vs CTR C6. n >11, 6, 10.

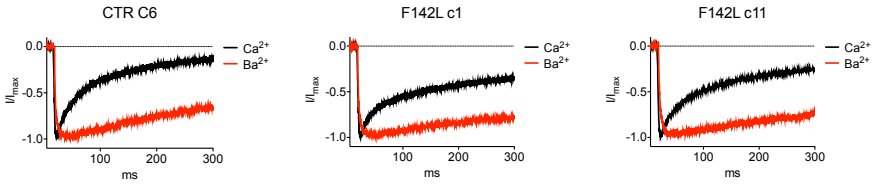

Figure 2.9: Examples of I_{CaL} (black) and I_{BaL} (red) recorded in CTR C6 and F142 clones. Traces were normalized to current peak. A minor CDI is observed for F142L clones, with a significant portion of I_{CaL} still not inactivated after 300 ms.

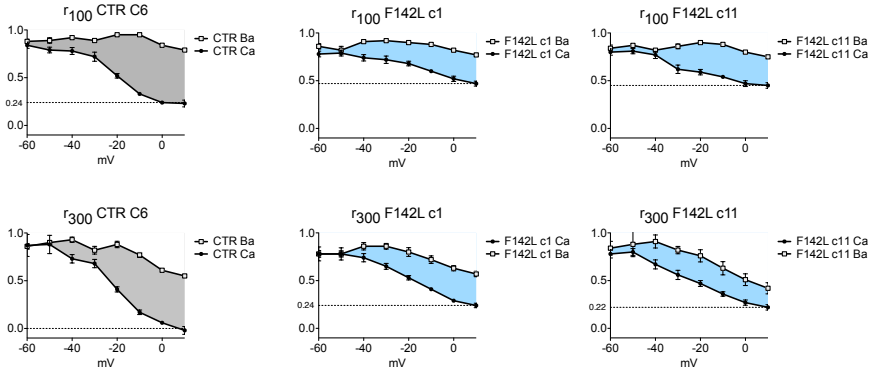

Figure 2.10: CDI for CTR C6 (dark grey) and F142L clones (blue). r_{100} and r_{300} are presented as the area between I_{BaL} (strictly voltage-dependent inactivation) and I_{CaL} (both voltage and Ca^{2+}-dependent inactivation). n = 11, 12, 13.

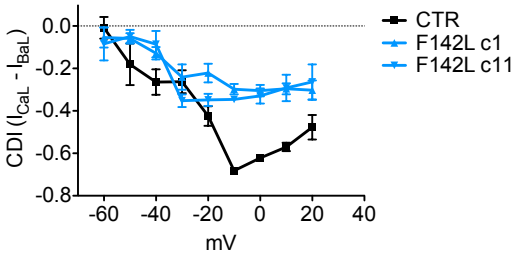

Figure 2.11: Analysis of CDI obtained by subtracting I_{BaL} r_{100} values to I_{CaL} ones in matched cells for CTR C6 (black) and F142L clones (blue). n >5, 6, 6.

2.4.3.2 Action Potentials

We then evaluated the effect of F142L mutation on AP shape and parameters. Figure 2.12 shows the comparison between native AP and AP recorded injecting a human I_{K1} model via DC. Average values are summarized in tables 3.3 and 2.7 respectively for native and DC APs.
Native AP evidenced a depolarized E_{diast} at all cycle lengths. APD_{90} and APD at 50% of repolarization phase (APD_{50}) values at 0.5 Hz, 1 Hz, 2 Hz were prolonged in F142L cells compared to CTR C6; APD_{50}/APD_{90} was not changed by stimulation frequency in both groups (figure 2.14).

The injection of I_{K1} with DC dramatically changed AP contour, making it representative of the AP shape of adult human cardiomyocytes [19](figure 2.12). Even at a physiological E_{diast}, F142L cells evidenced markedly prolonged APD_{90} and APD_{50} compared to CTR at pacing frequencies of 0.5 Hz, 1 Hz and 2 Hz (figure 2.13). No differences were observed at 3 Hz due to the fact that nearly 50% of F142L cells were significantly unable to adapt to this frequency compared to a value of 8% for CTR (figure 2.15); for this reason, comparison of APD values at 3 Hz has to be considered biased. Representative AP traces at 3 Hz stimulation are evidenced in figure 2.16. APD_{50}/APD_{90} was not altered by the frequency (figure 2.14). AP alternans at 2 Hz were absent in CTR and recorded in 20% of F142L hiPSC-CMs but without reaching statistical significance. Diastolic and peak I_{K1} densities were equal at all frequencies between CTR and F142L (figure 2.17). No changes were recorded in E_{diast} by increasing the stimulation frequencies.

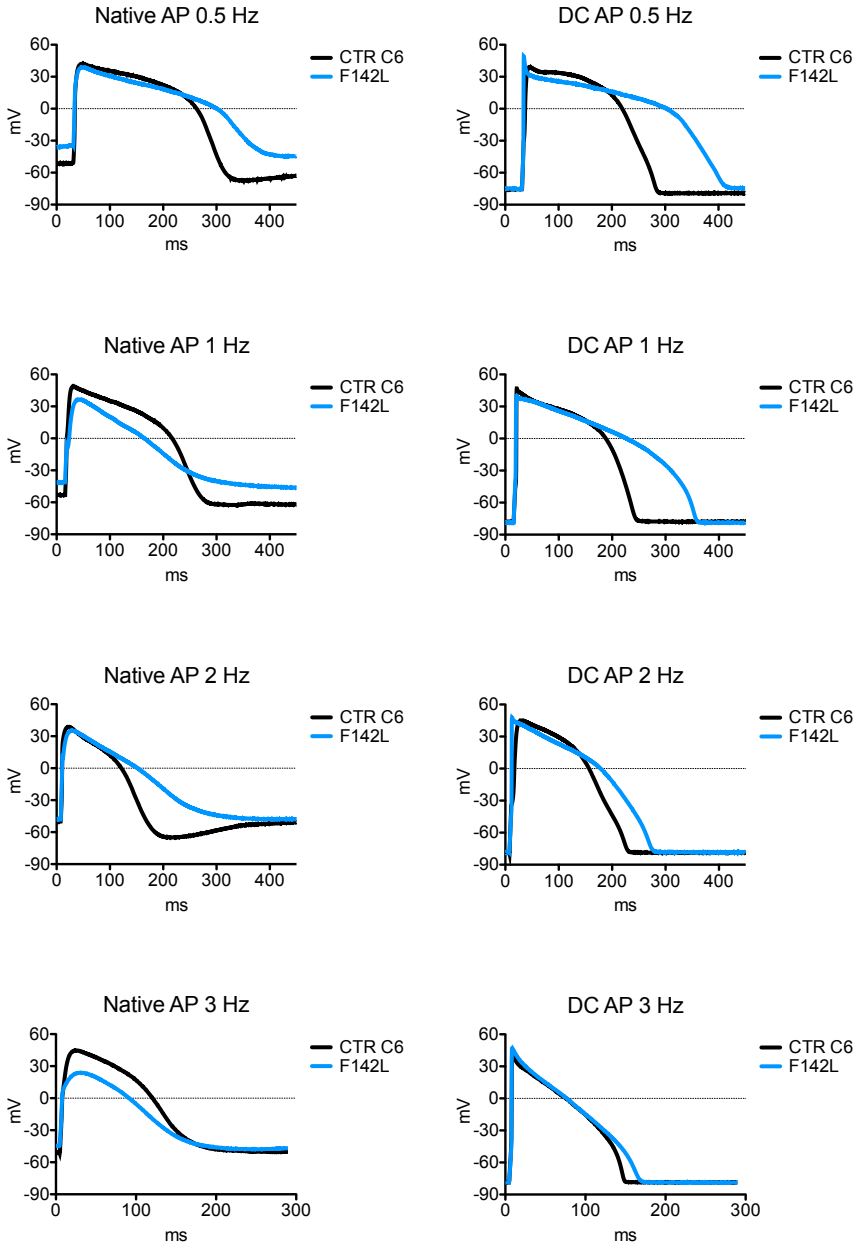

Figure 2.12: Native (*left*) and DC (*right*) APs recorded from CTR (black) and F142 (blue) hiPSC-CMs at stimulation frequencies of 0.5 Hz, 1 Hz, 2 Hz and 3 Hz. n >9, 13.

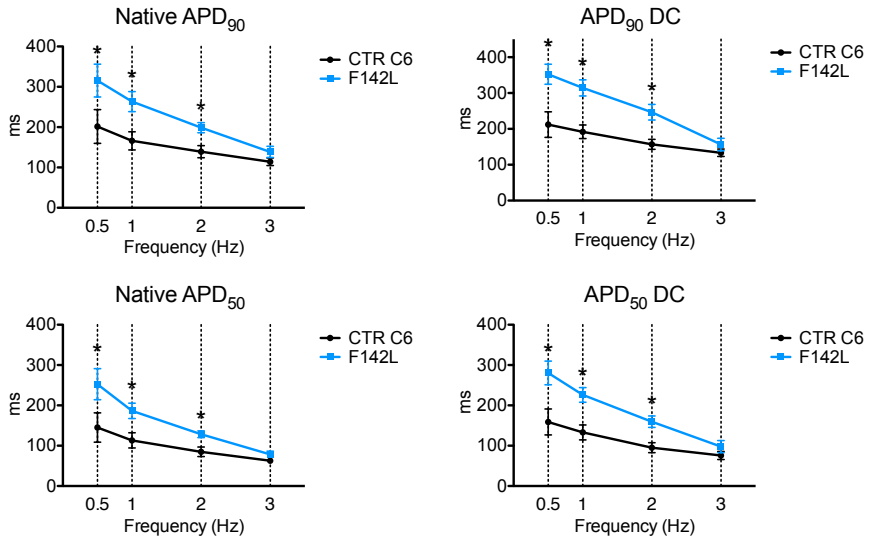

Figure 2.13: Average results from native (*left*) and DC (*right*) APs. The APD prolongation was clearly visible in both conditions. 3 Hz data points must be considered biased as half of cells did not adapt to the frequency. n >9, 13. ∗ = p <0.05 vs CTR.

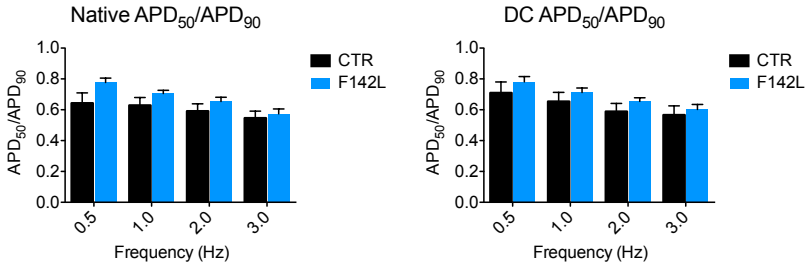

Figure 2.14: APD_{50}/APD_{90} analysis in native (*left*) and DC (*right*) conditions for CTR C6 (black) and F142L clones (blue) indicates that APD prolongation is uniform throughout the whole AP shape.

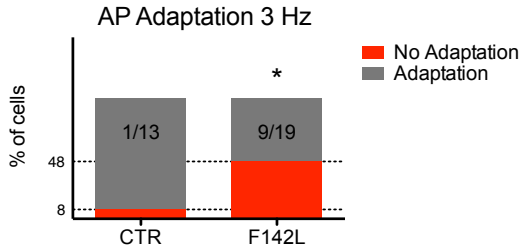

Figure 2.15: Statistics for AP adaptation to 3 Hz frequency. Half of F142L cells did not adapt to the fast frequency. ∗ = p <0.05 vs CTR.

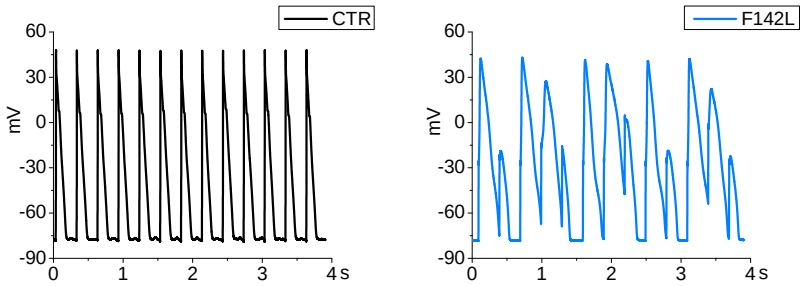

Figure 2.16: Representative DC APs at 3 Hz frequency in CTR (*left*, black) and F142L (*right*, blue) cells. Arrhythmic phenotype was evidenced in half F142L cells and is provoked by maladaptation to the high frequency.

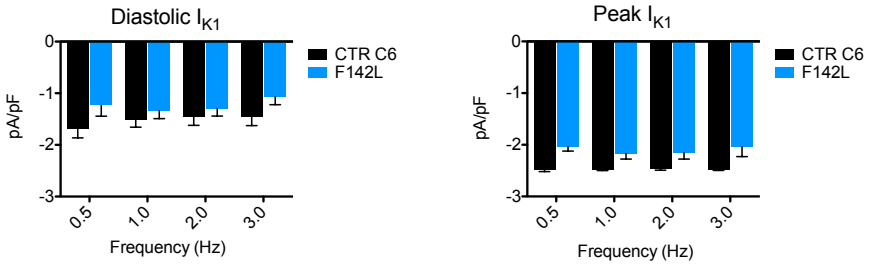

Figure 2.17: Peak and diastolic I_{K1} densities in DC experiments in CTR C6 (black) and F142L clones (blue). No differences were evidenced in these parameters at each frequency. n $>$9, 11.

Parameter	CTR				F142L			
	Frequency (Hz)							
	0.5	1	2	3	0.5	1	2	3
E_{diast} (mV)	-49.5 ± 3.4	-47.4 ± 2.7	-48.3 ± 3.0	-46.8 ± 3.7	-38.4 ± 3.3	-42.8 ± 1.8	-44.1 ± 1.9	-47.2 ± 2.4
APD_{50} (ms)	145.2 ± 36.4	113.3 ± 18.9	84.9 ± 11.9	62.9 ± 7.4	252.6 ± 38.4∗	186.6 ± 18.9∗	128.6 ± 8.4∗	78.59 ± 7.8
APD_{90} (ms)	201.6 ± 41.8	166.1 ± 22.5	139.0 ± 15.0	114.1 ± 9.3	315.6 ± 40.6∗	263.3 ± 24.8∗	198.7 ± 12.5∗	138.7 ± 13.8
APD_{50}/APD_{90}	0.64 ± 0.06	0.63 ± 0.05	0.59 ± 0.04	0.55 ± 0.04	0.77 ± 0.02	0.71 ± 0.02	0.65 ± 0.03	0.57 ± 0.03
Peak amplitude (mV)	40.3 ± 3.9	39.0 ± 3.4	37.8 ± 2.8	29.2 ± 4.3	41.16 ± 4.3	36.2 ± 2.5	33.9 ± 2.9	29.2 ± 4

Table 2.6: Native AP parameters for CTR C6 and F142 clones at 4 pacing frequencies. $*$ = p $<$0.05 vs CTR.

Parameter	CTR				F142L			
	Frequency (Hz)							
	0.5	1	2	3	0.5	1	2	3
E_{diast} (mV)	-75.3 ± 1.1	-75.1 ± 1.4	-76.4 ± 0.7	-76.6 ± 0.5	-70.3 ± 4.3	-74.1 ± 2.4	-73.9 ± 2.6	-73.4 ± 4.1⊗
APD_{50} (ms)	159.0 ± 32.2	133.0 ± 18.6	95.1 ± 12.2	75.8 ± 10.1	280.6 ± 29.4∗	226.0 ± 18.0∗	159.5 ± 14.1∗	97.8 ± 15.1⊗
APD_{90} (ms)	211.9 ± 35.7	191.9 ± 18.9	157.0 ± 13.9	133.5 ± 10.1	352.4 ± 27.8∗	314.4 ± 22.6∗	246.5 ± 21.7∗	156.4 ± 17.3⊗
APD_{50}/APD_{90}	0.70 ± 0.07	0.65 ± 0.06	0.59 ± 0.05	0.57 ± 0.06	0.78 ± 0.03	0.71 ± 0.03	0.65 ± 1.8	0.60 ± 0.03⊗
Peak amplitude (mV)	43.6 ± 2.1	43.7 ± 1.7	41.8 ± 1.7	38.0 ± 2.7	47.7 ± 1.8	42.9 ± 1.5	39.2 ± 1.8	37.3 ± 3.6⊗
I_{K1} peak (pA/pF)	-2.49 ± 0.03	-2.48 ± 0.01	-2.47 ± 0.02	-2.47 ± 0.02	-2.03 ± 0.08∗	-2.16 ± 0.1	-2.15 ± 0.12	-2.03 ± 0.2⊗
I_{K1} diastolic (pA/pF)	-1.69 ± 0.2	-1.50 ± 0.2	-1.45 ± 0.2	-1.45 ± 0.2	-1.23 ± 0.2	-1.33 ± 0.15	-1.29 ± 0.1	-1.07 ± 0.15⊗

Table 2.7: DC AP parameters for CTR C6 and F142 clones at 4 pacing frequencies. ∗ = p <0.05 vs CTR. ⊗ = data obtained only from cells adapting to 3 Hz.

2.4.3.3 Ca^{2+}-handling

Intracellular Ca^{2+} measurements were performed to investigate whether CaM mutation may alter Ca^{2+}-handling in addition to the effects on I_{CaL}. These measurements were performed only on F142L c1. Diastolic Ca^{2+} levels were not changed by the mutation (figure 2.19). Ca^{2+} transients evidenced a characteristic shape, constituted by early and late peaks, corresponding respectively to the beginning and the end of the depolarizing voltage step. The early peak, representative of Ca^{2+} influx via I_{CaL}, was increased in F142L clones. The late peak, instead, describes a slow and progressive cytosolic Ca^{2+} increment, probably due to the sum of NCX effect and Ca^{2+} release from the SR; this parameter was not changed between groups. Caffeine-induced Ca^{2+} release, an index of SR Ca^{2+} content, was not changed by the mutation. As a direct consequence, fractional release from the SR was increased.

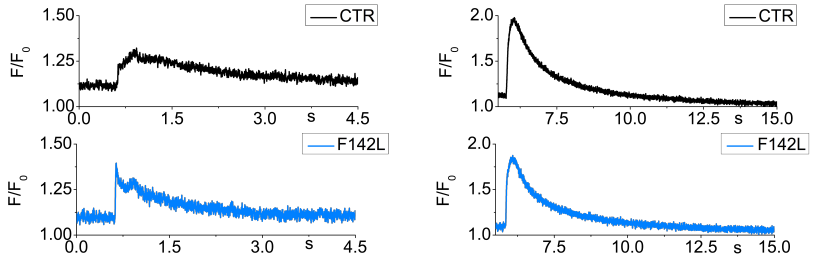

Figure 2.18: Representative traces for Ca^{2+} dynamics. Calcium transients evoked by a depolarizing step (*left*) or 10 mM caffeine (*right*) in CTR and F142L.

2.4.4 EB contraction

Qualitative analysis of EB contraction evidenced profound differences between groups. F142L clones were characterized by a pronounced plateau phase with a markedly slow decay. On the opposite, CTR clones exhibited rapid rise and decay of EB shortening.

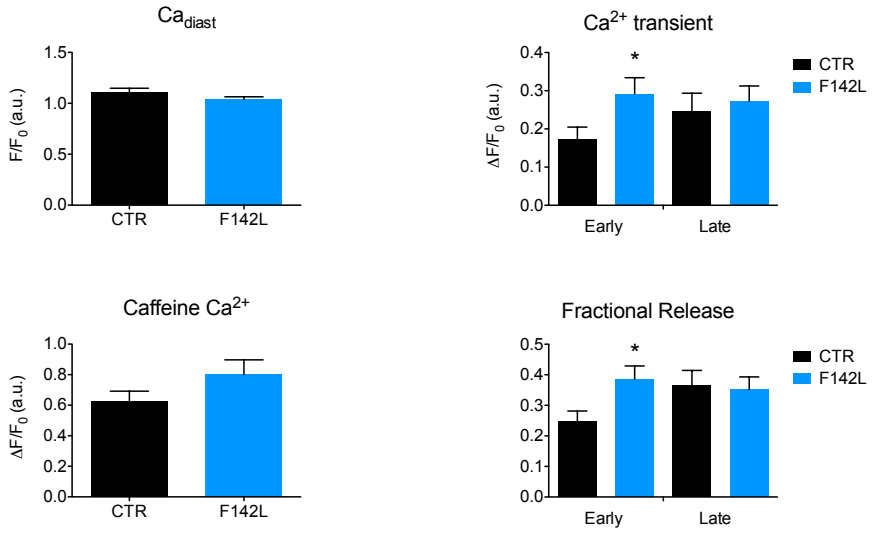

Figure 2.19: *Statistics for Ca^{2+} dynamics:* diastolic Ca^{2+} (Ca_{diast}), Ca^{2+} transients, SR content and Fractional Release were tested in CTR C6 (black) and F142L clones (blue). $*$ = p <0.05 vs CTR.

As visible in figure 2.20, the spontaneous beating rate was slower for mutated clones.

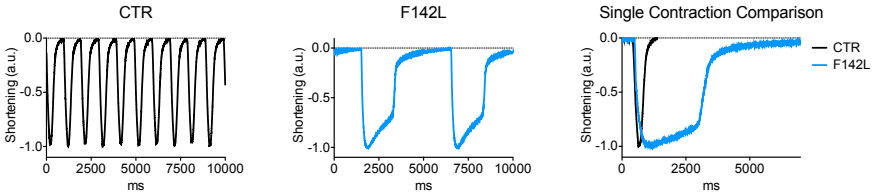

Figure 2.20: Representative spontaneous contractions recorded in CTR (black) and F142L (blue) EBs. RR intervals were 0.8 s for CTR and 5 s for F142L.

2.4.5 MultiElectrode Array

MEA studies confirmed AP data, evidencing a strong prolongation of QT interval for F142 clones (figures 2.21 and 2.22). Moreover, RR interval was also significantly longer in F142L.

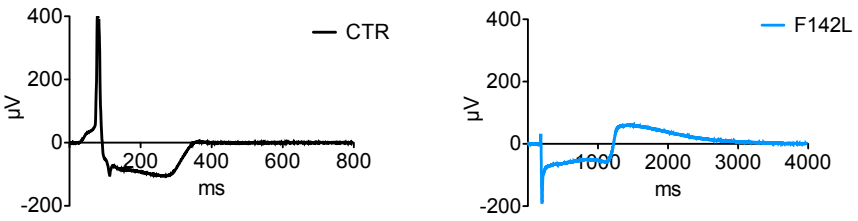

Figure 2.21: Representative MEA traces from CTR (*left*, black) and F142L (*right*, blue) EB. A strong QT interval prolongation is clearly visible.

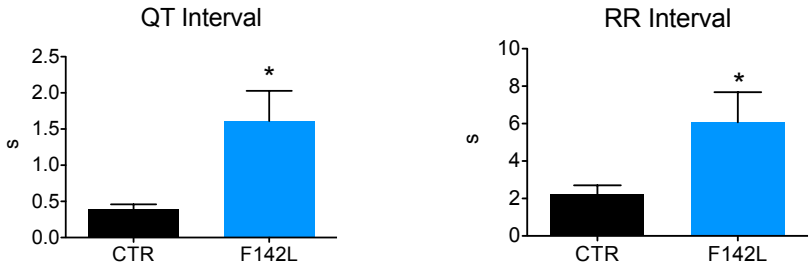

Figure 2.22: Average QT (*left*) and RR (*right*) intervals obtained from CTR (black) and F142L (blue) EBs indicate a strong QT prolongation and a slower RR for mutated clones. $*$ = p $<$0.05 vs CTR. n = 10, 8.

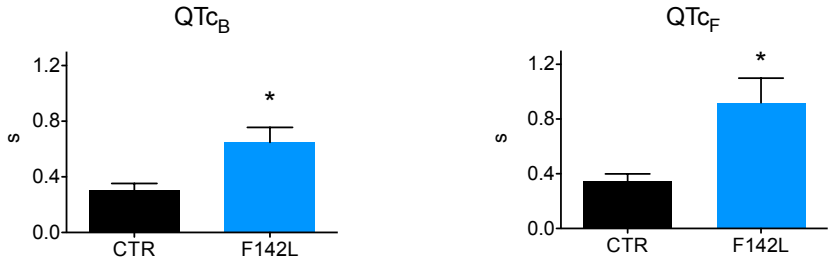

Figure 2.23: Average QT_c obtained from CTR (black) and F142L (blue) EBs indicate a strong QT interval prolongation for mutated clones. QT intervals were adjusted with both Bazett's (QTc_B) and Fridericia's (QTc_F) corrections. $*$ = p $<$0.05 vs CTR.

Linear relationships between QT and RR intervals were observed for both CTR and F142L in basal conditions. The slope factor was increased in F142L, indicating that, independently by the RR, QT intervals were prolonged (figure 2.24). The weight of the RR interval on QT_c calculation was analyzed in basal conditions (figures 2.25). We observed that Bazett's correction was more effective in making QT independent from RR in both CTR and F142L. Flat QT_c-RR relationships were indeed obtained for CTR, while much steeper linear regression plots were produced for F142L in basal condition. Then, we performed the same correlations under ISO stimulation. ISO shortened QT and RR intervals (figure 2.26) starting from the lower dose (50 nM). The effects on QT_c were modest but still significant with Bazett's correction (figure 2.27). Under ISO stimulation, CTR maintained its flat QT-RR or QT_c-RR relationships, while F142L clones displayed steeper relationships (figure 2.28).

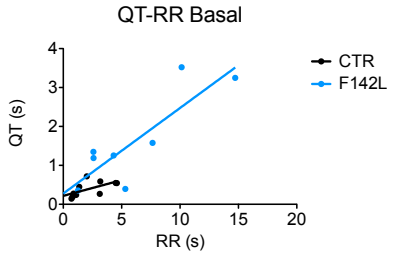

Figure 2.24: QT-RR relationships for CTR (black) and F142L (blue) in basal conditions. Lines indicate linear regression fittings. CTR: r^2: 0.3874, 1/slope: 12.36, p = 0.06. F142L: r^2: 0.7176, 1/slope: 4.55 p = 0.008.

2.5 Discussion

The present work provides a functional characterization of a LQTS mutation in patient-specific hiPSC-CMs. This gave new informations on the arrhythmogenic mechanisms underlying F142L muta-

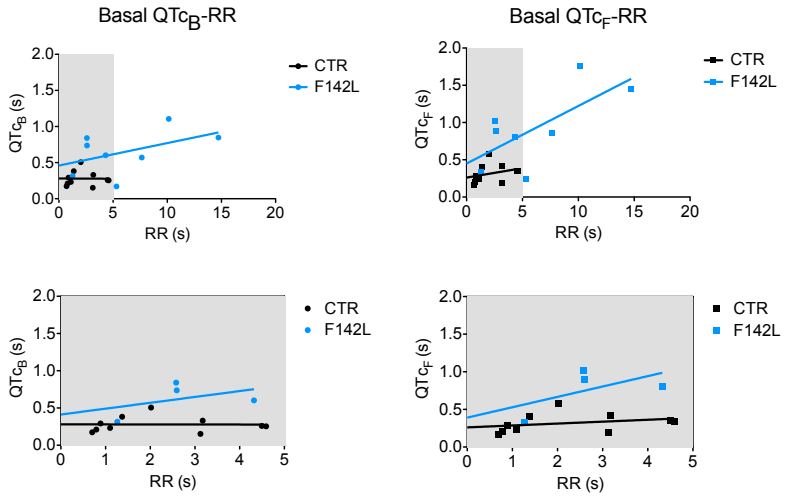

Figure 2.25: *Top:* QT_c-RR relationships for CTR (black) and F142L (blue). The area in gray indicated the RR interval, magnified in the insets. *Bottom:* magnification of RR intervals to evidence flat linear fit. CTR: QTc_B: r^2: 0.00006, 1/slope: -1781, p = 0.98. F142L: QTc_B: r^2: 0.1882, 1/slope: 12.72 p = 0.56.

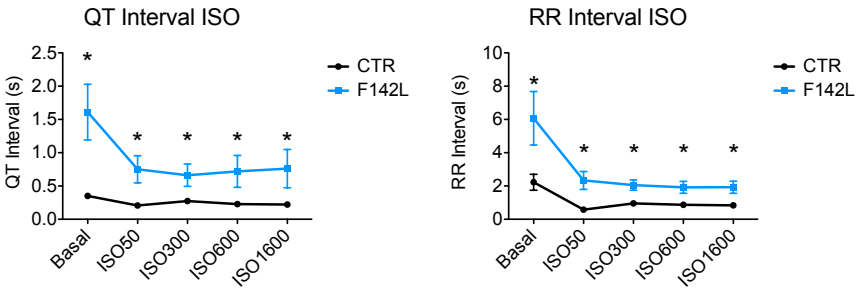

Figure 2.26: Effect of ISO on QT and RR intervals in CTR (black) and F142L (blue) EBs. Mutated EBs had prolonged QT and slower RR intervals. $*$ = p <0.05 vs CTR.

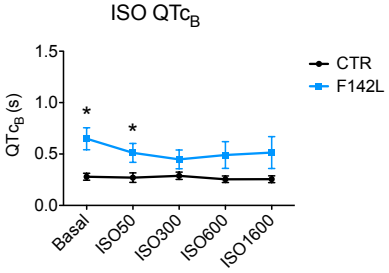

Figure 2.27: Effects of ISO on QTc_B at different ISO concentrations. $*$ = p <0.05 vs CTR.

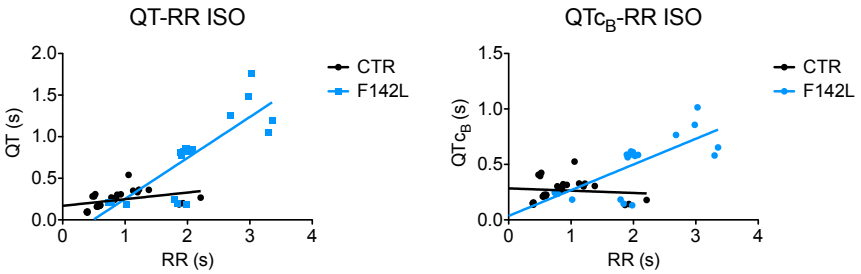

Figure 2.28: QT-RR and QT_c-RR correlations under ISO stimulation for CTR (black) and F142L (blue). Flat linear fit was obtained for CTR, while steeper fit emerged from F142L. *CTR:* QT: r^2: 0.1444, 1/slope: -12.52, p = 0.0383. QTc_B: r^2: 0.01006, 1/slope: -48.58, p = 0.5980. *F142L:* QT: r^2: 0.7094, 1/slope: 2.031, p <0.0001. QTc_B: r^2: 0.5518, 1/slope: 4.315, p = 0.0001.

tion in CALM1 gene.

2.5.1 Clone consistency

Two hiPSC-CMs control lines were generated from healthy donors: C6 and HAK. Divergences were evidenced in I_{CaL} magnitude and steady state activation. These differences could be explained by analyzing the source of primary explants: C6 line was derived from skin fibroblasts of a white female, while HAK line was obtained by reprogramming keratinocytes of an afro-american male. It is well described that gender and ethnicity may be key player in setting channels expression and AP duration [23]. Similar situations might be avoided by choosing a close relative as a donor; unfortunately, in our situation this was not possible since the patient was adopted and family data were poor and inconsistent. Complete consistency was found instead in I_{CaL} biophysical parameters as window current and CDI. This clearly indicates that, although current densities were different, both CTR lines possessed adult $Ca_v1.2$ with an identical Ca^{2+}-CaM-dependent regulation. Furthermore, APD in both native and DC conditions were alike, supporting a strong homogeneity within the CTR phenotype.

Two clones of the same patients were used for F142L mutation: c1 and c11. A complete clone consistency emerged from the data, indicating a strong reliability and reproducibility of the reprogramming process from a single biopsy.

2.5.2 Mutation effects

Many aspects of the clinical phenotype of F142L mutation were recreated in vitro with patient-specific hiPSC-CMs. Here we generated a functional characterization of this mutation in isolated cells on Ca^{2+} channels biophysics and AP. In addition, MEA studies were performed on EB.

Our results showed that F142L mutation acts firstly by altering the Ca^{2+}-binding properties of CaM, generating a strong decrease in CDI without altering I_{CaL} magnitude. Ca^{2+} transient were increased and, since the SR Ca^{2+} content was unchanged, the increment observed in fractional release was probably derived from an enhanced Ca^{2+} influx from I_{CaL}. In addition, some speculation can be made on the mechanisms extruding Ca^{2+} from cytosol, as an increased NCX or PMCA activity or protein expression. However, these hypotheses have not been tested yet.

The peculiar shape of voltage-induced Ca^{2+} transient raises questions regarding the Ca^{2+}-induced Ca^{2+} release mechanism in these cells. The presence of a slow rising fluorescence throughout the depolarizing step suggests that a substantial portion of Ca^{2+} transients in hiPSC-CMs depends from nuclear or IP_3 mediated Ca^{2+} stores, as previously demonstrated for cardiomyocytes derived from hESC [24]. In addition, the hiPSC-CMs membrane lacks of t-tubules, generating delays in excitation-contraction coupling and asynchronous Ca^{2+} transients.

The incomplete steady-state inactivation and an increase in window current constitute undoubtedly a potentially arrhythmogenic

background. From a theoretical point of view, these alterations would imply the presence of arrhythmogenic event in AP. Surprisingly, we did not observed such events. We evaluated AP in native condition and with the injection of an *in silico* I_{K1}: the former had a depolarized E_{diast}, which translates in incomplete channels recruiting and deranged AP profile, while the latter's AP contour fitted with data from human cardiomyocytes [19]. Remarkably, the APD prolongation generated by F142L mutation was observed in both native and DC conditions at three frequencies without experiencing arrhythmogenic events; this is in strong contrast with the results emerged by overexpressing CALM1 transcript in heterologous system [13][14], which evidenced the presence of EAD in patched cells at 0.5 Hz stimulation. Furthermore, the presence of AP alternans was reduced in our cell population compared to the heterologous system [13]. Cell adaptation to high frequencies was highly unbalanced in F142L, with half of the cells incapable of adapting to 3 Hz. This matches clinical data reporting that F142L patient experienced arrhythmic event and fibrillation mainly during tachycardia.

In addition, since I_{Ks} trafficking and regulation are mediated by Ca^{2+}-CaM interaction with $K_v7.1$ [25], it is reasonable to hypothesize also variations in I_{Ks} expression and magnitude, leading to a worsening of the phenotype; since I_{Ks} channels accumulate in the open state at high frequency [26], the derangement observed, as in our case, should be more visible at short cycle lengths. However, more experiments are still required to assess the real contribution of I_{Ks} during repolarization in this cells.

The pathological phenotype of the mutation was also confirmed with MEA. F142L EB exhibited a slower beating rate, consistently with the clinic, since the patient was described experiencing nocturnal bradycardia. The QT/RR relationship, evaluated in basal

conditions, was steeper for F142L than CTR, indicating a bigger QT interval prolongation as RR increases, in accordance with the recorded AP data; furthermore, linear regression fits converged at fast frequencies, perfectly in accordance with our AP data at 3 Hz. The normalization of QT intervals with both Bazett's and Fridericia's correction evidenced a relationship still dependent on the frequency; this also indicated that F142L EB had a greater QT variability, a situation that may compromise myocardial repolarization in the whole heart. Restricting the RR values below 5 seconds, thus excluding EB with abnormal RR values, produced a flatter QT_c-RR relationship for both groups, where a modest variation of RR does not strongly alter QT interval.

Under ISO stimulation, the situation was profoundly different. A strong ISO sensitivity was evidenced by both groups, starting from the lower dose, on both QT and RR intervals. This compacted all RR values within a 5 seconds interval, thus allowing the comparison with basal condition in the same range. Here, QT/RR and QT_c/RR relationships were maintained flat for CTR, suggesting that changes in beating frequency do not alter significantly the repolarization duration. On the opposite, F142L clones displayed a pronounced slope in the fittings ($r^2 = 0.71$ and 0.55, respectively for QT and QTc_B, $p < 0.0001$), as a consequence of the much prolonged RR interval, whose influence on QT interval cannot be excluded by Bazett's correction. This produces two phenomena: 1) a slight increase in RR interval, e.g. as a consequence of β-blockers, produces important and dangerous QT prolongation in F142L; 2) at fast frequencies (i.e. <1 s), the QT_c of F142L group drifted below CTR values, indicating that a shorter QT_c should be required in order to compensate RR changes. However, the QT_c shortening is prevented by the failing CDI mechanism, generating the lack of adaptation to fast frequencies observed in isolated cells with DC.

Overall, these data recapitulate the pathological phenotype experienced by the patient and described the inability of adapt to fast frequencies as main arrhythmogenic mechanism for F142L mutation.

2.6 Acknowledgements

For the electrophysiological characterizations, I am grateful to Dr. Marcella Rocchetti, for expert support and advices on experimental design, measurements and data interpretation. F142L patient data were provided by Dr. Lia Crotti, who firstly discovered and published a clinical report of CALM F142L mutation [10]. iPS were generated by Dr. Lisa Dreizehnter and coworkers, in the laboratory of Dr. Alessandra Moretti, at the Technische Universität München (TUM), Munich, Germany. EB were cultured and dissociated by Dr. Manuela Mura, working in the laboratory of Dr. Massimiliano Gnecchi, at the IRCCS Policlinico San Matteo, Pavia, Italy. Expert support was provided by Dr. Peter J. Schwartz, working at the Istituto Auxologico Italiano. The in silico I_{K1} model for DC studies was kindly provided by Dr. Stefano Severi, working at the University of Bologna, Cesena, Italy. The DC technique was implemented in our laboratory by the effort of Dr. Claudia Altomare, Dr. Marcella Rocchetti, Mr. Gaspare Mostacciuolo and Dr. Chiara Bartolucci (University of Bologna, Cesena, Italy). I am grateful to Prof. Antonio Zaza for suggestions on experimental design and data interpretation.

2.7 References

1. Park, H. Y. *et al.* Conformational changes of calmodulin upon Ca2+ binding studied with a microfluidic mixer. *Proc. Natl. Acad. Sci. U.S.A.* **105,** 542–547 (Jan. 2008).
2. Simms, B. A., Souza, I. A. & Zamponi, G. W. A novel calmodulin site in the Cav1.2 N-terminus regulates calcium-dependent inactivation. *Pflugers Arch - Eur J Physiol* **466,** 1793–1803 (Sept. 2014).
3. Coleman, N. *et al.* New positive Ca2+-activated K+ channel gating modulators with selectivity for KCa3.1. *Molecular Pharmacology* **86,** 342–357 (Sept. 2014).
4. Oruganti, S. R., Edin, S., Grundström, C. & Grundström, T. CaMKII targets Bcl10 in T-cell receptor induced activation of NF-κB. *Mol. Immunol.* **48,** 1448–1460 (July 2011).
5. Pachuau, J., Li, D.-P., Chen, S.-R., Lee, H.-A. & Pan, H.-L. Protein kinase CK2 contributes to diminished small conductance Ca2+-activated K+ channel activity of hypothalamic pre-sympathetic neurons in hypertension. *J. Neurochem.* **130,** 657–667 (Sept. 2014).
6. Fischer, T. H. *et al.* Ca(2+) /calmodulin-dependent protein kinase II equally induces sarcoplasmic reticulum Ca(2+) leak in human ischaemic and dilated cardiomyopathy. *Eur. J. Heart Fail.* n/a–n/a (Sept. 2014).
7. O'Day, D. H. & Myre, M. A. Calmodulin-binding domains in Alzheimer's disease proteins: extending the calcium hypothesis. *Biochemical and Biophysical Research Communications* **320,** 1051–1054 (Aug. 2004).

8. Martinez, J., Moeller, I., Erdjument-Bromage, H., Tempst, P. & Lauring, B. Parkinson's disease-associated alpha-synuclein is a calmodulin substrate. *Journal of Biological Chemistry* **278,** 17379–17387 (May 2003).

9. Niebroj-Dobosz, I, Kornguth, S, Schutta, H. S. & Siegel, F. L. Elevated calmodulin levels and reduced calmodulin-stimulated calcium-ATPase in Duchenne progressive muscular dystrophy. *Neurology* **39,** 1610–1614 (Dec. 1989).

10. Crotti, L. *et al.* Calmodulin Mutations Associated With Recurrent Cardiac Arrest in Infants. *Circulation* **127,** 1009–1017 (Mar. 2013).

11. Makita, N. *et al.* Novel calmodulin mutations associated with congenital arrhythmia susceptibility. *Circ Cardiovasc Genet* **7,** 466–474 (Aug. 2014).

12. Nyegaard, M. *et al.* Mutations in calmodulin cause ventricular tachycardia and sudden cardiac death. *Am. J. Hum. Genet.* **91,** 703–712 (Oct. 2012).

13. Limpitikul, W. B. *et al.* Calmodulin mutations associated with long QT syndrome prevent inactivation of cardiac L-type Ca2+ currents and promote proarrhythmic behavior in ventricular myocytes. *Journal of Molecular and Cellular Cardiology* **74,** 115–124 (Sept. 2014).

14. Yin, G. *et al.* Arrhythmogenic calmodulin mutations disrupt intracellular cardiomyocyte Ca2+ regulation by distinct mechanisms. *Journal of the American Heart Association* **3,** e000996–e000996 (June 2014).

15. Hwang, H. S. *et al.* Divergent regulation of ryanodine receptor 2 calcium release channels by arrhythmogenic human calmodulin missense mutants. *Circulation Research* **114,** 1114–1124 (Mar. 2014).

16. Moretti, A. *et al.* Patient-specific induced pluripotent stem-cell models for long-QT syndrome. *N Engl J Med* **363,** 1397–1409 (Oct. 2010).

17. Takahashi, K. *et al.* Induction of Pluripotent Stem Cells from Adult Human Fibroblasts by Defined Factors. *Cell* **131,** 861–872 (Nov. 2007).

18. Wilders, R. Dynamic clamp: a powerful tool in cardiac electrophysiology. *J. Physiol. (Lond.)* **576,** 349–359 (Oct. 2006).

19. O'Hara, T., Virág, L., Varró, A. & Rudy, Y. Simulation of the undiseased human cardiac ventricular action potential: model formulation and experimental validation. *PLoS Comput Biol* **7,** e1002061 (May 2011).

20. Zaza, A, Rocchetti, M, Brioschi, A, Cantadori, A & Ferroni, A. Dynamic Ca2+-induced inward rectification of K+ current during the ventricular action potential. *Circulation Research* **82,** 947–956 (May 1998).

21. Lin, R. J., Bettencourt, J., Wha Ite, J., Christini, D. J. & Butera, R. J. Real-time experiment interface for biological control applications. *Conf Proc IEEE Eng Med Biol Soc* **2010,** 4160–4163 (2010).

22. Liang, P. *et al.* Drug screening using a library of human induced pluripotent stem cell-derived cardiomyocytes reveals disease-specific patterns of cardiotoxicity. *Circulation* **127,** 1677–1691 (Apr. 2013).

23. Makkar, R. R., Fromm, B. S., Steinman, R. T., Meissner, M. D. & Lehmann, M. H. Female gender as a risk factor for torsades de pointes associated with cardiovascular drugs. *JAMA* **270,** 2590–2597 (Dec. 1993).

24. Satin, J. *et al.* Calcium Handling in Human Embryonic Stem Cell-Derived Cardiomyocytes. *Stem Cells* **26,** 1961–1972 (Aug. 2008).

25. Shamgar, L. Calmodulin Is Essential for Cardiac IKS Channel Gating and Assembly: Impaired Function in Long-QT Mutations. *Circulation Research* **98,** 1055–1063 (Apr. 2006).

26. Rocchetti, M *et al.* Rate dependency of beta-adrenergic modulation of repolarizing currents in the guinea-pig ventricle. *J. Physiol. (Lond.)* **574,** 183–193 (July 2006).

Chapter 3

KCNQ1^{Y111C} mutation

3.1 Acronyms

WT	wild type
AS	asymptomatic
S	symptomatic
SNP	single nucleotide polymorphisms
C$_m$	membrane capacitance

3.2 Introduction

Congenital LQTS is a rare genetical disease characterized by a pathological prolongation of the QT interval in the ECG [1]. Its most common form is the LQT1, which accounts for almost 40% of total LQTS cases [1][2] and is described as a loss of function of the repolarizing current I_{Ks} as a consequence of a mutation in KCNQ1 [3]. Two main mechanisms are found responsible for I_{Ks} reduction in patients with KCNQ1 mutation: 1) the assembly of mutant subunit not transported properly to cell membrane [4] and 2) defective channels formed and transported to plasma membrane [5]. These

conditions make the patient prone to EAD with subsequent TdP via reentry [1]. The majority of LQT1 patients experience cardiac events in conditions promoting the sympathetic activity as stress or physical activity [1][3]. This happens since I_{Ks} is boosted in response to β-adrenergic stimulation via protein kinase A (PKA) phosphorilation to counterbalance the concurring increase in Ca^{2+} current [6]. The $KCNQ1^{Y111C}$ is a mutation localized in the N-terminus of KCNQ1. It has been firstly identified in a 36-year-old woman experiencing more than 30 episodes of seizures, starting at 3 years of age, induced by physical and emotional stress [7]. Y111C mutation in the N-terminus of KCNQ1 has been associated to the autosomal dominant form of LQTS (RWS). It has been been extensively described in vivo as descendent from a single founder population in Sweden and it was enriched thanks to the mild clinical phenotype and the extremely low incidence of life-threatening cardiac events before β-blocker therapy [8]. In contrast, in vitro experiments evidenced instead a very severe phenotype for this LQTS mutation [9][10], causing a defective plasma membrane trafficking of $K_v7.1$, with consequent accumulation of mutated channels in the endoplasmic reticulum. Coexpression with KCNE1 did not increase the expression of functional channels, even in the presence of the fusion protein in which the two subunits are concatenated [10]. In addition, a strong dominant negative effect was evidenced when co-transfected with $KCNQ1^{WT}$ [11]. The divergence between in vivo and in vitro data raises the hypothesis that potential genetic modifiers may co-segregate with the mutation to blunt or worsen the effects of the Y111C polymorphism. As previously pointed out for the severe $KCNQ1^{A341V}$ mutation, functional in vitro experiments do not translate directly into clinical reality [5]. The analysis of the origin of $KCNQ^{Y111C}$ mutation revealed that it was introduced in Sweden 600 years ago and suffered from a strong regional founder

effect in addition to the mutation enrichment made possibile by the mild clinical phenotype. For these reasons, the KCNQ1^{Y111C} founder population is considered an important asset for future genetic and clinical studies [8]. One possible strategy to include the genetic background component in the study of LQTS mutations, is the use of patient-specific hiPSC-CMs.

In this study, we evaluated two relatives with KCNQ1^{Y111C} mutation experiencing an opposite clinical phenotype. The father (asymptomatic (AS)), healthy, with a normal QT_c interval and its son (symptomatic (S)), experiencing clinical events due to a pathological QT_c prolongation (table 3.1).

The aims of this study were: 1) to evaluate the effects of Y111C mutation in KCNQ1 with patient-specific hiPSC-CMs; 2) to analyze genotype-phenotype correlation in two relatives with the same mutation but different clinical outcomes.

3.3 Methods

3.3.1 Patients

Both subjects are Italian and diagnosed by Dr. Lia Crotti, M.D., at Policlinico San Matteo IRCCS, Pavia. The father, 58 years old, has a normal QT_c interval (417 ms). He is not in therapy and did not experience cardiac events. The son, 14 years old, has a pathological QT_c prolongation (490 ms) and experienced 1 episode of syncope with sphincter release during stress; he is currently under β-blockers (table 3.1). Both patients had also been screened for other common single nucleotide polymorphisms (SNP) which may explain the different phenotype. No SNP were detected in the 3'UTR of KCNQ1^{Y111C} and in CALM1 gene. The mother was healthy and not carrying the KCNQ1^{Y111C} mutation.

	asymptomatic (AS)	symptomatic (S)
Family	Father	Son
Age (years)	58	14
Heart rate (bpm)	62	78
Clinical events	none	1 episode of syncope
Therapy	none	Propranolol

Table 3.1: Characteristics of the two relatives involved in this study.

3.3.2 hiPSC-CMs generation

hiPSC-CMs were generated as previously published [12, 13]. Briefly, skin biopsies were collected from AS and S patients and expanded in DMEM 10% FBS. Dermal fibroblasts were then replated in multiwell dishes and transfected by retrovirus containing Yamanaka's factors: SOX2, KLF4, OCT4, c-Myc [14]. After 14 days, putative iPS clones were manually picked and expanded in feeder-free system with mTeSR^{TM} medium. IMR-90 human cell line was used as control. Before inducing cardiac differentiation, iPS were dissociated into single cells with accutase and seeded in matrigel®-coated dishes. RPMI medium was supplemented in different days with: ROCK inhibitor (Y27632, 5 μM) and GSK-β inhibitor (CHIR99021, 12 μM) on day 1; Wnt-signaling inhibitor (IWP1, 5 μM) on day 4; on day 7, RPMI-B27 was added and beating areas started to appear from day 9. After 30 days from differentiation induction, beating areas were manually dissected and used for MEA or dissociated for single cell studies. Dissociated hiPSC-CMs were tested positive for α-actinin, tropomyosin and troponin-T with GFP-conjugated Antibodies (Ab) (figure 3.1).

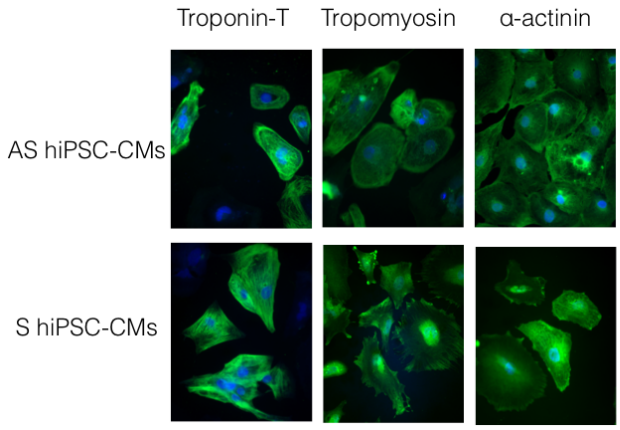

Figure 3.1: AS and S isolated hiPSC-CMs stained with GFP-Ab for α-actinin (*Top*), tropomyosin (*center*) and troponin-T (*bottom*).

3.3.3 Patch Clamp

3.3.3.1 I_{Ks} measurements

I_{Ks} measurements were performed in Tyrode's solution containing (mM): 140 NaCl, 4 KCl, 2 $CaCl_2$, 1.2 $MgCl_2$, 5 HEPES and 11 D-glucose, adjusted to pH 7.4 with NaOH. 1μM E-4031 and 1 μM nifedipine were added to avoid the interference of I_{Kr} and I_{CaL} respectively. I_{Ks} was isolated as the tail current sensitive to 1 μM HMR-1556. Pipette solution contained (mM): 110 K-aspartate, 23 KCl, 3 $MgCl_2$, 2 $CaCl_2$, 5 HEPES-KOH, 5 EGTA-KOH, 5 ATP Na^+-salt, 5 phosphocreatine, 0.4 GTP Na^+ salt; pH was adjusted to 7.3 with KOH. A standard voltage clamp protocol was used to evoke I_{Ks}: from an holding potential of -40 mV, 5 depolarizing step of 3750 ms with 20 mV increments were applied at a CL of 8 s. I_{Ks} measurements were performed at 36 °C.

3.3.3.2 AP measurements

Native AP were measured with patch clamp in current clamp configuration at four different frequencies (Hz): 0.5, 1, 2, 3. hiPSC-CMs

have low native expression of I_{K1}, with a consequent depolarized E_{diast} and the presence of automatic activity in ventricular-like cells. We addressed this issue with a DC approach [15]: a human I_{K1} numerical model, derived from the Rudy-O'Hara model [16], was injected into hiPSC-CMs. To better suit the experimental design, E_{rev} was set to -80 mV. Furthermore, G_{max} required a 10 fold increase to match the I_{K1} profile of adult myocytes [17]. The model was injected using the Real-Time eXperiment Interface (RTXI, [18]) running on Ubuntu 10.04 LTS, paired with an A/D converter (BNC-2120, National Instruments, Austin, TX, USA). AP experiments were performed in Tyrode's solution at 36 °C with a pipette solution containing (mM): 110 K-aspartate, 23 KCl, 3 $MgCl_2$, 5 HEPES-KOH, 0.5 EGTA-KOH, 5 ATP Na^+-salt, 5 phosphocreatine, 0.4 GTP Na^+ salt; pH was adjusted to 7.3 with KOH.

3.3.4 Transfection

hiPSC-CMs were transfected with 0.5 μg of fusion plasmid (VSV-KCNE1-KCNQ1) containing a VSV-tag, wild type (WT) KCNE1 and KCNQ1 WT ($KCNQ1^{WT}$) or mutated ($KCNQ1^{Y111C}$). Cells were transfected with Fugene (2 μL / 35 mm Petri dish, Promega). GFP was used to facilitate the choice of transfected cells for patch clamp experiments. Currents were evaluated 72 h after transfection.

3.3.5 MultiElectrode Array

A 256-electrode MEA (Multi Channel Systems) was used for the recordings. The medium contained DMEM supplemented with: 5% FBS, 1 mM Na^+-pyruvate, 1:1000 penicillin / streptomycin, 1:1000 L-glutamine, 1:100 Insulin-Transferrin-Selenium (ITS), 1:100 NEAA. All substances were added with a pipette in volumes of 5 μL. A 100 fold dilution was used considering a MEA chamber volume of

500 μL [19]. Steady state was reached within 5 minutes of recording. Data analysis was performed with MC Rack, MC Data Tool (Multi Channel Systems) and pClamp suite (Molecular Devices). QT interval were obtained from the first peak of depolarization, indicating the phase 0 of the AP, to the last repolarizing peak, correspondent to the AP repolarization. QT_c intervals were calculated with standard Bazett's (QTc_B) and Fridericia's (QTc_F) corrections.

3.3.6 Statistics

Student's t-test or ANOVA for unpaired measurements were applied as appropriate to test for significance between means. Post hoc comparison between individual means was performed by Bonferroni's or Dunn's multiple comparison tests. Average data are expressed and plotted as the mean ± standard error of the mean. Statistical significance was defined as $p < 0.05$ (n.s., not significant). The sample size for each experiment is specified in the respective figure legend. All the analyses were performed with GraphPad Prism v5.0c for Mac.

3.4 Results

3.4.1 Cellular parameters

The average C_m was 63.2 ± 9.1 pF for CTR, 71.2 ± 6.6 pF for AS, 64.3 ± 9.1 pF for S. The vast majority of cells tested evidenced a ventricular-like phenotype, while only a few atrial or nodal-like were observed. Details on cell number and experimental groups are indicated in figure legends.

3.4.2 Patch Clamp

3.4.2.1 Native I_{Ks}

The magnitude of native I_{Ks} was tested in the three cell populations. Albeit very small, I_{Ks} was measurable only in CTR cells. Its density was consistent with previous data from hiPSC-CMs ([20]). As expected from an LQT1 mutation, I_{Ks} density was significantly reduced in AS and S cells (figure 3.3). No differences emerged from the comparison of I_{Ks} from AS and S cells.

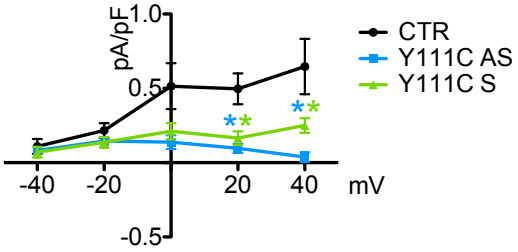

Figure 3.2: Native I_{Ks} tail current for CTR (black), AS (blue) and S (green). n = 10, 8, 10. $*$ = p <0.05 vs CTR.

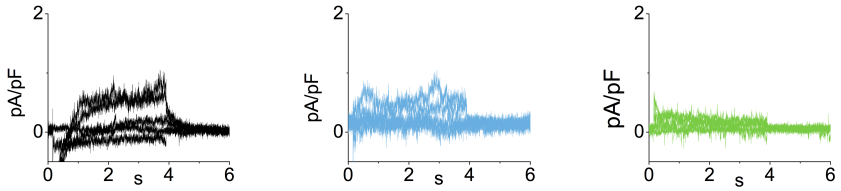

Figure 3.3: Native I_{Ks} tail current for CTR (black), AS (blue) and S (green).

3.4.2.2 Transfected I_{Ks}

Since I_{Ks} densities were too low to allow a discrimination between AS and S, we performed transfection experiments with KCNQ1^{WT} and KCNQ1^{Y111C} plasmids (figures 3.4 and 3.5). Firstly, CTR hiPSC-CMs were transfected with KCNQ1^{WT}, evidencing a strong

increase in I_{Ks} density. The transfection with KCNQ1^{Y111C} did not produce an increase of I_{Ks} over the native level.

Then, we transfected AS hiPSC-CMs with both plasmids. We observed an increased in tail current similar to CTR when transfected with KCNQ1^{WT} (Current density at +40 mV for transfection with KCNQ1^{WT}: 3.4 ± 0.9 pA/pF for CTR vs 1.9 ± 1.3 pA/pF for AS, n.s.). I_{Ks} remained low when cells were transfected with KCNQ1^{Y111C}. We then transfected S cells with the same plasmids. The mutated channel did not increase current density over the baseline, which was already negligible. We observed a small increase in I_{Ks} when transfecting the WT channel. This increase remained much weaker than the one observed in CTR cells transfected with the same plasmid (Current density at +40 mV for transfection with KCNQ1^{WT}: 3.4 ± 0.9 pA/pF for CTR vs 0.65 ± 0.2 pA/pF for S, p <0.05).

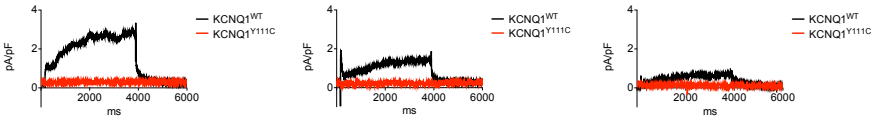

Figure 3.4: Transfected KCNQ1^{WT} (black) and KCNQ1^{Y111C} (red), measured at +40 mV, in CTR (*left*), AS (*center*) and S (*right*).

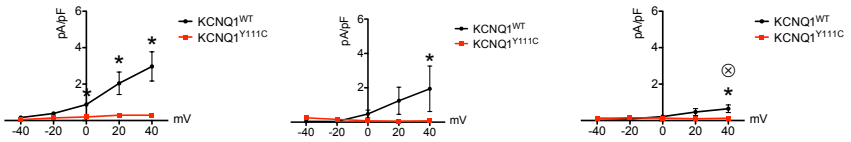

Figure 3.5: Transfection of KCNQ1^{WT} and KCNQ1^{Y111C} in CTR (*left*, n = 12, 11), AS (*middle*, n = 4, 6) and S (*right*, n = 9, 6) hiPSC-CMs. ∗ = p <0.05 vs KCNQ1^{WT}. ⊗ = p < 0.05 vs CTR.

3.4.2.3 Dynamic Clamp

AP were evaluated in both native and DC conditions (figure 3.6).

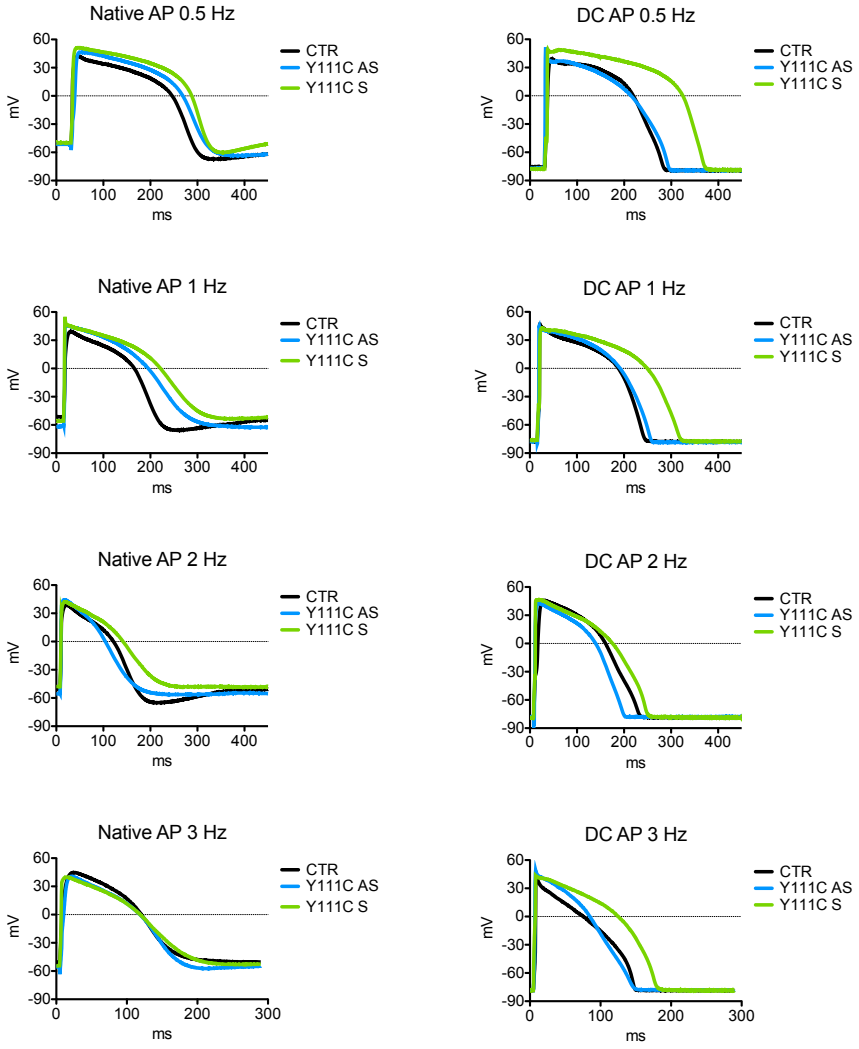

Figure 3.6: Representative native (*left*) and DC (*right*) APs recorded from CTR (black), AS (blue) and S (green) hiPSC-CMs at stimulation frequencies of 0.5 Hz, 1 Hz, 2 Hz and 3 Hz.

E_{diast} was depolarized in native condition, leading to incomplete channel recruiting and data biasing. Differences were evidenced in APD_{50} and APD_{90} in this condition (figure 3.7). APD_{50}/APD_{90} was equal in all groups at low frequency, with a significant increase at 3 Hz. The injection of computational simulated I_{K1} shifted E_{diast} towards -80 mV, confirming the LQTS phenotype for S, compared to APD from CTR and AS groups (figure 3.8). APD_{50}/APD_{90} ratio evidenced a significant increase starting from 1 Hz. (figure 3.9).

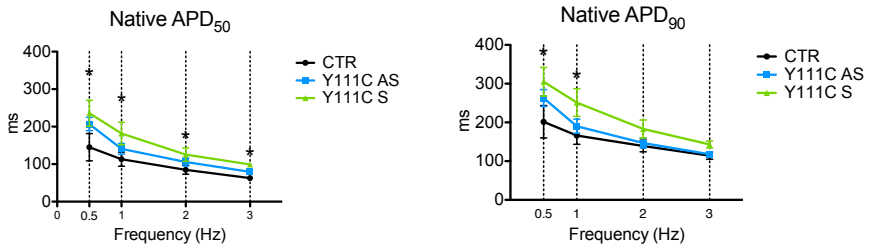

Figure 3.7: Average results from Native APD_{50} and APD_{90} for CTR (black), AS (blue) and S (green). APD prolongation is confirmed in S group, compared to CTR. n >9, 10, 12.

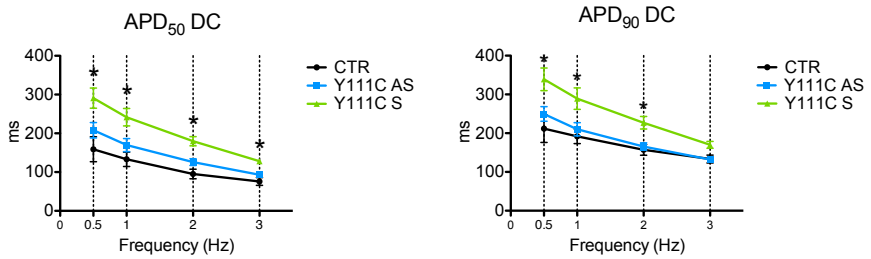

Figure 3.8: Average results from DC APD_{50} and APD_{90} in CTR (black), AS (blue) and S (green). A statistical significance was present in almost all conditions. n >9, 10, 12. $*$ = p <0.05 vs CTR.

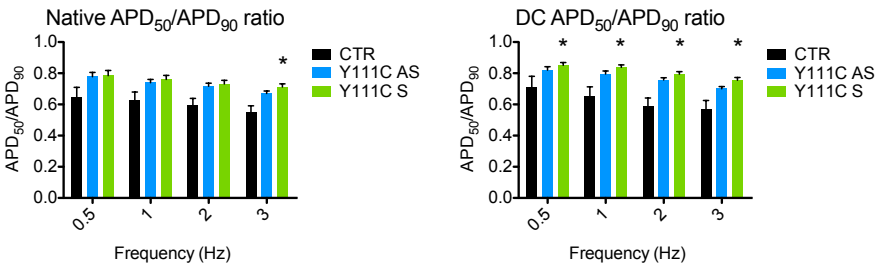

Figure 3.9: Average results from APD_{50}/APD_{90} ratio in CTR (black), AS (blue) and S (green). n >9, 10, 12. $*$ = p <0.05 vs CTR.

	Frequency (Hz)	E_{diast} (mV)	APD_{50} (ms)	APD_{90} (ms)	APD_{50}/APD_{90}	Peak amplitude (mV)
CTR	0.5	-49.5 ± 3.4	145.2 ± 36.4	201.6 ± 41.8	0.64 ± 0.06	40.3 ± 3.9
	1	-47.4 ± 2.7	113.3 ± 18.9	166.1 ± 22.5	0.63 ± 0.05	39.0 ± 3.4
	2	-48.3 ± 3.0	84.9 ± 11.9	139.0 ± 15.0	0.59 ± 0.04	37.8 ± 2.8
	3	-46.8 ± 3.7	62.9 ± 7.4	114.1 ± 9.3	0.55 ± 0.04	29.2 ± 4.3
Y111C AS	0.5	-52.0 ± 2.8	207.0 ± 17.7	262.9 ± 21.8	0.78 ± 0.03	45.2 ± 1.9
	1	-51.5 ± 3.0	140.9 ± 18.1	190.2 ± 18.1	0.74 ± 0.02	42.6 ± 2.7
	2	-51.7 ± 2.9	105.8 ± 10.7	146.7 ± 12.6	0.71 ± 0.02	39.9 ± 3.1
	3	-52.9 ± 2.1	79.4 ± 5.8	117.8 ± 7.0	0.67 ± 0.02	37.8 ± 1.9
Y111C S	0.5	-50.1 ± 2.3	235.9 ± 34.3∗	298.9 ± 41.3∗	0.78 ± 0.03	47.8 ± 4.1
	1	-50.1 ± 2.8	181.7 ± 30.2∗	239.6 ± 40.0∗	0.76 ± 0.03	46.6 ± 2.6
	2	-47.8 ± 3	125.5 ± 17.8	172.0 ± 24.6	0.73 ± 0.02	42.9 ± 2.2
	3	-51.3 ± 1.6	99.1 ± 7.0	139.1 ± 8.7	0.71 ± 0.02∗	42.0 ± 3.7

Table 3.2: Native AP parameters for CTR, Y111C AS and Y111C S clones at 4 pacing frequencies. $*$ = p <0.05 vs CTR.

	Frequency (Hz)	E_{diast} (mV)	APD_{50} (ms)	APD_{90} (ms)	APD_{50}/APD_{90}	Peak amplitude (mV)	I_{K1} peak (pA/pF)	I_{K1} diastolic (pA/pF)
CTR	0.5	-75.3 ± 1.1	159.0 ± 32.2	211.9 ± 35.7	0.70 ± 0.07	43.6 ± 2.1	-2.49 ± 0.03	-1.69 ± 0.2
	1	-75.1 ± 1.4	133.0 ± 18.6	191.9 ± 18.9	0.65 ± 0.06	43.7 ± 1.7	-2.48 ± 0.01	-1.50 ± 0.2
	2	-76.4 ± 0.7	95.1 ± 12.2	157.0 ± 13.9	0.59 ± 0.05	41.8 ± 1.7	-2.47 ± 0.02	-1.45 ± 0.2
	3	-76.6 ± 0.5	75.8 ± 10.1	133.5 ± 10.1	0.57 ± 0.06	38.0 ± 2.7	-2.47 ± 0.02	-1.45 ± 0.2
Y111C AS	0.5	-75.7 ± 0.9	208.0 ± 19.7	249.6 ± 18.8	0.82 ± 0.02	42.7 ± 2.3	-1.99 ± 0.08	-1.42 ± 0.2
	1	-77.1 ± 0.7	169.7 ± 16.7	210.12 ± 17.0	0.80 ± 0.01	42.4 ± 2.4	-2.18 ± 0.06	-1.06 ± 0.2
	2	-77.9 ± 0.4	125.8 ± 8.6	165.5 ± 9.5	0.76 ± 0.01	41.7 ± 2.7	-2.32 ± 0.03	-0.9 ± 0.1
	3	-77.5 ± 0.4	93.0 ± 5.9	132.2 ± 6.4	0.70 ± 0.01	40.8 ± 1.9	-2.36 ± 0.02	-1.1 ± 0.1
Y111C S	0.5	-77.1 ± 0.5	290.7 ± 26.0∗	339.1 ± 29.1∗	0.85 ± 0.01∗	47.6 ± 2.0	-2.10 ± 0.06	-1.1 ± 0.1
	1	-77.7 ± 2.8	241.7 ± 27.5∗	289.2 ± 27.5∗	0.84 ± 0.03∗	47.7 ± 1.2	-2.05 ± 0.06	-0.9 ± 0.2
	2	-78.1 ± 0.2	179.7 ± 11.9∗	227.0 ± 16.1∗	0.79 ± 0.02∗	46.5 ± 1.3	-2.21 ± 0.06	-0.8 ± 0.08
	3	-77.7 ± 1.6	128.3 ± 7.0∗	170.1 ± 8.9∗	0.76 ± 0.02∗	44.1 ± 1.1	2.20 ± 0.09	-0.99 ± 0.08

Table 3.3: DC AP parameters for CTR, Y111C AS and Y111C S clones at 4 pacing frequencies. ∗ = p <0.05 vs CTR.

3.4.3 MultiElectrode Array

MEA analysis confirmed the APD prolongation. QT intervals were prolonged only in S, compared to AS and CTR. In addition, RR intervals were found equal in all the three groups (figures 3.10 and 3.11).

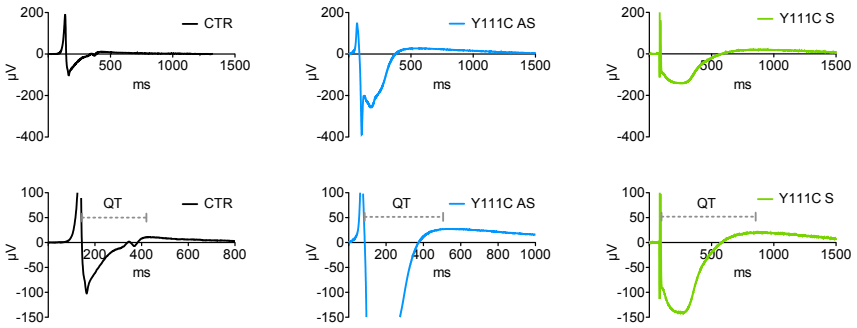

Figure 3.10: Representative MEA traces from CTR (*left*, black), AS (*center*, blue) and S (*right*, green) EB. QT interval prolongations are magnified in the insets.

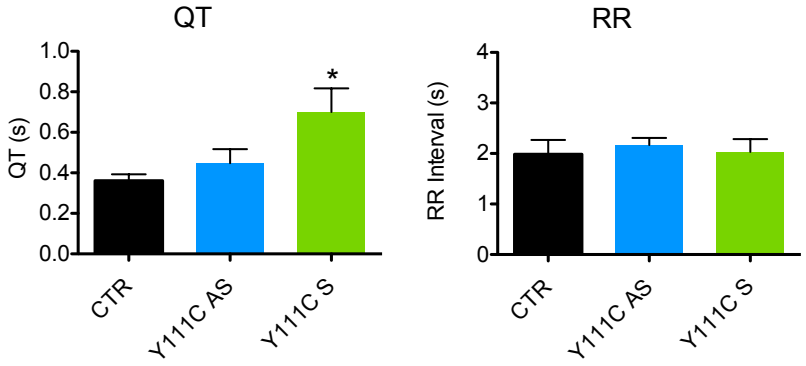

Figure 3.11: QT (*left*) and RR (*right*) intervals for CTR (black), AS (blue) and S (green). n = 23, 10, 11. ∗ = p <0.05 vs CTR.

QT-RR relationships for the three groups evidenced that the QT interval increases linearly with the RR interval (figure 3.12). To make QT independent from RR, we corrected QT intervals with Bazett's (QTc_B) and Fridericia's (QTc_F) methods; QT_c intervals

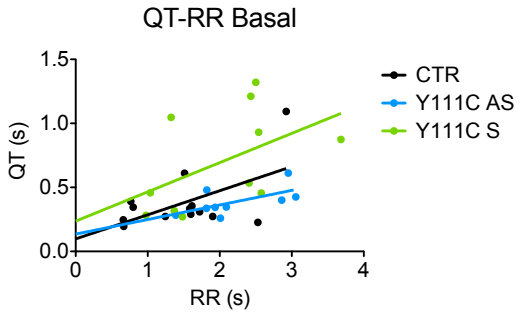

Figure 3.12: QT-RR relationships for CTR (black), AS (blue), S (green). Lines indicates linear regression fit with the following results: CTR: r^2: 0.3042, 1/slope: 5.318, p = 0.0507. AS: r^2: 0.3874, 1/slope: 8.788, p = 0.0734. S: r^2: 0.2480, 1/slope: 4.378, p = 0.1191. n = 23, 10, 11.

were longer only in S, confirming the QT prolongation previously observed (figure 3.13). Furthermore, we obtained a flat QT_c-RR relationship as a consequence of the corrections (figure 3.14); this indicates that both correction methods perfectly cleared QT values from the influence of RR intervals.

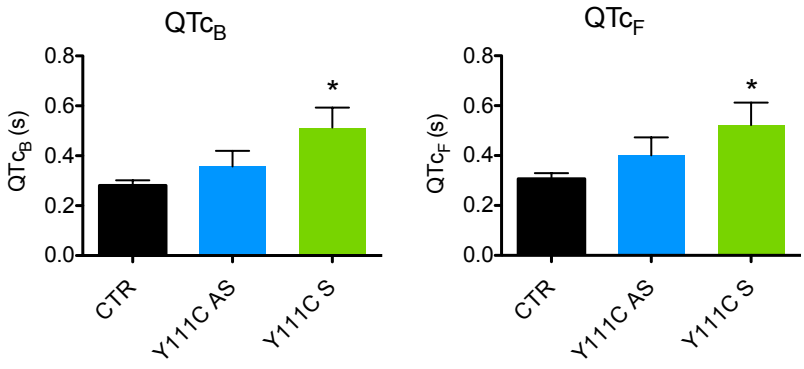

Figure 3.13: Average QT_c obtained from CTR (black), AS (blue) and S (green) indicate a strong QT interval prolongation S. QT intervals were adjusted with both Bazett's (QTc_B) and Fridericia's (QTc_F) corrections. $*$ = p <0.05 vs CTR. n = 23, 10, 11.

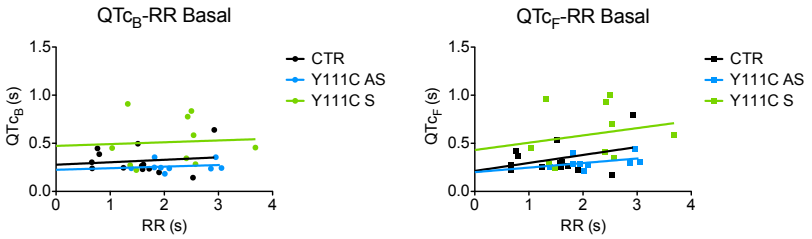

Figure 3.14: QTc-RR relationships for CTR (black), AS (blue), S (green). Lines indicates linear regression fit with the following results: QTc_B *(Left)*: CTR: r^2: 0.01644, 1/slope: 39.08, p = 0.6763. AS: r^2: 0.02908, 1/slope: 60.75, p = 0.6609. S: r^2: 0.003721, 1/slope: 52.98, p = 0.8671. QTc_F *(Right)*: CTR: r^2: 0.01644, 1/slope: 12.05, p = 0.2474. AS: r^2: 0.1525, 1/slope: 21.12, p = 0.2987. S: r^2: 0.04468, 1/slope: 13.19, p = 0.5577. n = 23, 10, 11.

3.5 Discussion

In this study we evaluated the effects of KCNQ1^{Y111C} mutation with patient-specific hiPSC-CMs. Previous data on heterologous system evidenced a strong loss of function effect for this mutation leading to a >75% decrease in I_{Ks} density [10]. However, clinical data did not match this observation, with patients showing a mild LQTS phenotype characterized by a small incidence of life-threatening cardiac events [21]. As previously reported for the KCNQ1^{A341V} mutation, this discrepancy can be explained with the presence of genetic factors influencing the severity of the disease. In this context, the use of patient-specific hiPSC-CMs represent an improvement towards the correspondence between in vitro and clinical data. In addition, the presence of the complete genetic background of patients may help in defining the role of modifying factors in the Swedish LQT1 population.

Our data were focused on the characterization of KCNQ1^{Y111C} mutation in hiPSC-CMs.

The native AP of hiPSC-CMs was not considered as reliable. A highly depolarized diastolic potential and the presence of automatic activity in ventricular cells, typical of immature cells, should be considered pathological conditions as in adult myocytes. To

compensate this, we implemented a computational model of human I_{K1} injected in real time with the patch clamp technique. This did hyperpolarize E_{diast} and prevented automatic activity. DC allows channels to work in the physiological range typical of adult myocytes, strongly increasing the reliability of AP measurements. In both native and DC conditions, the AP experiments were strongly consistent with clinical data, evidencing the LQTS phenotype only in S hiPSC-CMs. This was also confirmed by MEA in beating clusters, with a strong QT prolongation observed only for S EB. In addition, no differences in AS and S compared with CTR were found in RR intervals, accordingly to a normal sinus rhythm in both patients. This has to be considered a strong evidence of the correlation between in vitro and clinical data. Differently from other in vitro systems, our model strongly matches the clinical phenotype, increasing the importance and the validity of in vitro data.

Voltage-clamp measurements of native I_{Ks} confirmed the loss of function effect of the mutation. We observed differences in I_{Ks} magnitude between CTR and mutated hiPSC-CMs. In addition, the I_{Ks} density measured in CTR cells is perfectly comparable with previous experiments in Guinea Pigs [17], dogs and hiPSC-CMs [20]. However, possibly due to the small size of the current, it was extremely difficult to appreciate potential differences between the two patients.

Since $KCNQ1^{Y111C}$ channels are retained into citoplasm [10], we decided to further investigate the role of protein folding, degradation and trafficking machinery with transfection experiments. We transfected $KCNQ1^{Y111C}$ or $KCNQ1^{WT}$ in these cell populations. Accordingly to literature [9], experiments evidenced a huge reduction of I_{Ks} when $KCNQ1^{Y111C}$ was transfected in each group. In AS, $KCNQ1^{WT}$ generate a tail current totally comparable to CTR cells, indicating that the machinery for protein folding and degradation

is intact and fully functional. Surprisingly, in S, the transfection with KCNQ1^{WT} experienced a massive reduction in I_{Ks}, suggesting a potential derangement in protein folding or trafficking. We hypothesize this to be the main difference between AS and S, may indeed accounting for the different phenotype of the two patients.

Recent works suggested the importance of ion channels ubiquitylation in regulating their degradation and expression on cell membrane [22]. It has been demonstrated that the expression of repolarizing current I_{Ks}, I_{Kr} and I_{K1} is influenced by the activity of protein related to the ubiquitylation pathway. In particular, Kv7.1 protein levels are reduced by the activity of Nedd4-2 via binding to the PY domain on the channel [23]. Furthermore, even Kv11.1 was found to be under the control of Nedd4-2, which is able to diminish I_{Kr} density by ubiquitylating its PY domain [24].

At this point, there are three possible scenarios: 1) AS perfectly fit into the statistical data of Swedish LQT1 population, in which the majority of patients do not experience symptoms and, among them, a significant percentage possesses normal QT interval. In the same way, S may have its LQTS phenotype only derived by I_{Ks} loss of function. This hypothesis should be considered unlikely; first, because we observed a deranged I_{Ks} expression when S cells were transfected with KCNQ1^{WT}. Second, the two patients in this study are relatives and blaming the statistical variability of the population as a primary mechanism for these differences seems reckless. 2) AS patient owns a sort of rescue mechanism which restores normal values of QT_c, while S represents a clinical case consistent with the statistics of Swedish population. Again, this seems unlikely, since we demonstrated that S has an impaired protein trafficking even for KCNQ1^{WT}. 3) AS is consistent with part of the Swedish founder population which does not experience clinical symptoms, while S possesses an additional mechanism able to worsen the clinical phe-

notype. Based on our data, this seems to be the most plausible case since KCNQ1^{WT} transfection evidenced an impaired protein folding/trafficking machinery. Overall, these findings suggest the presence of an additive and concomitant pathological mechanism involving the protein regulation of other repolarizing ion channels.

Further experiments will clarify the role of genetic modifiers in the regulation of Kv11.1 expression between AS and S. In addition, I_{Kr} measurements will be performed to assess the contribution of ubiquitylation in regulating the activity of repolarizing currents.

In conclusion, our in vitro findings reproduced the major phenotypical traits observed in patients, suggesting that this model evidenced strong correlations between genotype and phenotypical traits. This confirms iPS as one of the best experimental currently available for the study of monogenic disease influenced by genetic background.

3.6 Acknowledgements

For the electrophysiological characterizations, I am grateful to Dr. Marcella Rocchetti, for expert support and advices on experimental design, measurements and data interpretation. Patients' data were provided by Dr. Lia Crotti. iPS were generated by Dr. Lee Yee-Ki and coworkers. In addition, she provided a molecular characterization of iPS and generated KCNQ1-KCNE1 plasmids. She is working in the laboratory of Prof. Hung-Fat Tse, at The University of Hong Kong, People's Republic of China. EB were cultured and dissociated by Dr. Manuela Mura, who performed also part of the transfections. She is working in the laboratory of Dr. Massimiliano Gnecchi, at the IRCCS Policlinico San Matteo, Pavia, Italy. Expert support was provided by Prof. Peter J. Schwartz, working at the Istituto Auxologico Italiano. The in silico I_{K1} model for DC

studies was kindly provided by Dr. Stefano Severi, working at the University of Bologna, Cesena, Italy. The DC technique was implemented in our laboratory by the effort of Dr. Claudia Altomare, Dr. Marcella Rocchetti, Mr. Gaspare Mostacciuolo and Dr. Chiara Bartolucci (University of Bologna, Cesena, Italy). I am grateful to Prof. Antonio Zaza for suggestions on experimental design and data interpretation.

3.7 References

1. Schwartz, P. J. *et al.* Genotype-phenotype correlation in the long-QT syndrome: gene-specific triggers for life-threatening arrhythmias. *Circulation* **103,** 89–95 (Jan. 2001).
2. Schwartz, P. J., Crotti, L. & Insolia, R. Long-QT syndrome: from genetics to management. *Circulation: Arrhythmia and Electrophysiology* **5,** 868–877 (Aug. 2012).
3. Crotti, L., Celano, G., Dagradi, F. & Schwartz, P. J. Congenital long QT syndrome. *Orphanet J Rare Dis* **3,** 18 (2008).
4. Bianchi, L *et al.* Mechanisms of I(Ks) suppression in LQT1 mutants. *Am J Physiol Heart Circ Physiol* **279,** H3003–11 (Dec. 2000).
5. Moss, A. J. *et al.* Clinical aspects of type-1 long-QT syndrome by location, coding type, and biophysical function of mutations involving the KCNQ1 gene. *Circulation* **115,** 2481–2489 (May 2007).
6. Lo, C. F. & Numann, R. Independent and exclusive modulation of cardiac delayed rectifying K+ current by protein kinase C and protein kinase A. *Circulation Research* **83,** 995–1002 (Nov. 1998).
7. Splawski, I *et al.* Spectrum of mutations in long-QT syndrome genes. KVLQT1, HERG, SCN5A, KCNE1, and KCNE2. *Circulation* **102,** 1178–1185 (Sept. 2000).
8. Winbo, A. *et al.* Origin of the Swedish long QT syndrome Y111C/KCNQ1 founder mutation. *Heart Rhythm* **8,** 541–547 (Apr. 2011).
9. Diamant, U. B. *et al.* Electrophysiological phenotype in the LQTS mutations Y111C and R518X in the KCNQ1 gene. *Journal of Applied Physiology* **115,** 1423–1432 (Nov. 2013).

10. Dahimène, S. *et al.* The N-terminal juxtamembranous domain of KCNQ1 is critical for channel surface expression: implications in the Romano-Ward LQT1 syndrome. *Circulation Research* **99,** 1076–1083 (Nov. 2006).

11. Dahimène, S. *et al.* The N-terminal juxtamembranous domain of KCNQ1 is critical for channel surface expression: implications in the Romano-Ward LQT1 syndrome. *Circulation Research* **99,** 1076–1083 (Nov. 2006).

12. Ho, J. C. Y. *et al.* Generation of induced pluripotent stem cell lines from 3 distinct laminopathies bearing heterogeneous mutations in lamin A/C. *Aging (Albany NY)* **3,** 380–390 (Apr. 2011).

13. Lai, W.-H. *et al.* ROCK inhibition facilitates the generation of human-induced pluripotent stem cells in a defined, feeder-, and serum-free system. *Cell Reprogram* **12,** 641–653 (Dec. 2010).

14. Takahashi, K. *et al.* Induction of Pluripotent Stem Cells from Adult Human Fibroblasts by Defined Factors. *Cell* **131,** 861–872 (Nov. 2007).

15. Wilders, R. Dynamic clamp: a powerful tool in cardiac electrophysiology. *J. Physiol. (Lond.)* **576,** 349–359 (Oct. 2006).

16. O'Hara, T., Virág, L., Varró, A. & Rudy, Y. Simulation of the undiseased human cardiac ventricular action potential: model formulation and experimental validation. *PLoS Comput Biol* **7,** e1002061 (May 2011).

17. Zaza, A, Rocchetti, M, Brioschi, A, Cantadori, A & Ferroni, A. Dynamic Ca2+-induced inward rectification of K+ current during the ventricular action potential. *Circulation Research* **82,** 947–956 (May 1998).

18. Lin, R. J., Bettencourt, J., Wha Ite, J., Christini, D. J. & Butera, R. J. Real-time experiment interface for biological control applications. *Conf Proc IEEE Eng Med Biol Soc* **2010,** 4160–4163 (2010).

19. Navarrete, E. G. *et al.* Screening drug-induced arrhythmia [corrected] using human induced pluripotent stem cell-derived cardiomyocytes and low-impedance microelectrode arrays. *Circulation* **128,** S3–13 (Sept. 2013).

20. Moretti, A. *et al.* Patient-specific induced pluripotent stem-cell models for long-QT syndrome. *N Engl J Med* **363,** 1397–1409 (Oct. 2010).

21. Winbo, A., Diamant, U.-B., Stattin, E.-L., Jensen, S. M. & Rydberg, A. Low incidence of sudden cardiac death in a Swedish Y111C type 1 long-QT syndrome population. *Circ Cardiovasc Genet* **2,** 558–564 (Dec. 2009).

22. Abriel, H. & Staub, O. Ubiquitylation of ion channels. *Physiology (Bethesda)* **20,** 398–407 (Dec. 2005).

23. Jespersen, T. *et al.* The KCNQ1 potassium channel is down-regulated by ubiquitylating enzymes of the Nedd4/Nedd4-like family. *Cardiovascular Research* **74,** 64–74 (Apr. 2007).

24. Albesa, M., Grilo, L. S., Gavillet, B. & Abriel, H. Nedd4-2-dependent ubiquitylation and regulation of the cardiac potassium channel hERG1. *Journal of Molecular and Cellular Cardiology* **51,** 90–98 (July 2011).

Chapter 4

Summary and conclusion

The present thesis work provides novel electrophysiological insights about two LQTS mutation.

The first study was focused on the F142L mutation in CALM1 gene, recently associated with an extremely severe arrhythmogenic phenotype in infants [1]. For the first time, this mutation was tested in patient-specific hiPSC-CMs, which allows the study of the mutation within patient's genotype. This study confirmed and reproduced the phenotype observe in clinics, with a particular focus on an increased arrhythmia susceptibility at high beating rates, which we account as the main arrhythmogenic mechanism for this patient. Furthermore, the perfect genotype-phenotype correlation observed will allow the creation and the development of new pharmacological strategies. Future experiments will be directed on the evaluation of pharmacological response to antiarrhythmic drugs in MEA. Specifically, a dose-response curve will be generated for two Ca^{2+} channel blockers of different classes (verapamil and amlodipine) to verify the in vitro effects of these drugs on mutated EB in MEA and hypothesize a potential translational application.

The second project unveiled the strong potential of patient-specific hiPSC-CMs in comparison with other in vitro experimen-

tal models[2]. Furthermore, the potential contribution of a genetic modifier in shaping the pathogenic phenotype of Y111C mutation in KCNQ1 was hypothesized [2][3]. This was made possible by recruiting two relatives bearing the same mutation but experiencing adverse clinical outcome. We demonstrated, by using hiPSC-CMs, that a gene diverse from the one causing the primary mutation may be able to influence the severity of the disease by acting on protein trafficking machinery from SR to the membrane. Further experiments will be focused on the investigation of protein folding/trafficking machinery in the both AS and S hiPSC-CMs lines.

Furthermore, in both works we clearly demonstrated that DC should be considered a powerful tool to overtake the immaturity of hiPSC-CMs in term of AP contour, at least until proper differentiation and maturation methods will be established.

MEA data, instead, confirmed that this platform is reliable and that could also be used for compound assays to predict the clinical and in vivo response to drugs. However, more efforts will be necessary to establish strong and reliable experimental protocols that could be implemented in the industry to speed up the preclinical drug selection process.

Translation relevances for this topic are huge. The possibility of study monogenic disease in a physiological environment comprehensive of patient's genotype will increase not only the accuracy of in vitro experimentations, but also the efficacy of clinical predictions. This approach can, indeed, provide clinicians useful information for therapy setting or correction, avoiding potential disastrous clinical outcomes. For these reasons, the use of hiPSC-CMs as a model for cardiac arrhythmias strongly enhances the reliability and predictability of in vitro experiments, paving the ground for new therapies and drug discovery assays.

4.1 References

1. Crotti, L. *et al.* Calmodulin Mutations Associated With Recurrent Cardiac Arrest in Infants. *Circulation* **127,** 1009–1017 (Mar. 2013).
2. Diamant, U.-B. *et al.* Electrophysiological phenotype in the LQTS mutations Y111C and R518X in the KCNQ1 gene. *J. Appl. Physiol.* **115,** 1423–1432 (Nov. 2013).
3. Winbo, A. *et al.* Origin of the Swedish long QT syndrome Y111C/KCNQ1 founder mutation. *Heart Rhythm* **8,** 541–547 (Apr. 2011).

Chapter 5

Published papers

1. Altomare C, Barile L, Rocchetti M, **Sala L**, Crippa S, Sampaolesi M, et al. *Altered functional differentiation of mesoangioblasts in a genetic myopathy.* 2013 Jan 1;17(3):419 - 28.

2. Rizzi R, Di Pasquale E, Portararo P, Papait R, Cattaneo P, Latronico MVG, Altomare C, **Sala L** et al. *Post-natal cardiomyocytes can generate iPS cells with an enhanced capacity toward cardiomyogenic re-differentation.* Cell Death Differ. 2012 Jul;19(7):1162 - 74.

3. Rocchetti M∗, **Sala L**∗, Rizzetto R, Staszewsky LI, Alemanni M, Zambelli V, et al. *Ranolazine prevents I_{NaL} enhancement and blunts myocardial remodelling in a model of pulmonary hypertension.* Cardiovascular Research. 2014 Oct 1;104(1):37 - 48 ∗ authors equally contributed to this work.

4. Rizzetto R, Rocchetti M, **Sala L**, Ronchi C, Villa A, Ferrandi M, et al. *Late sodium current (I_{NaL}) in pancreatic β-cells.* Pflugers Arch - Eur J Physiol. Springer Berlin Heidelberg; 2014 Sep 20:1 - 12.

5. Altomare C, Bartolucci C, **Sala L**, Rocchetti M, Mostacciuolo

G, Severi S, Zaza A *I_{Kr} impact on repolarization and its variability assessed by Dynamic-Clamp* Circulation: Arrhythmias and Electrophysiology; 2014 *Submitted on 19/11/2014.*